ISSN 1948-5204 (online)

World Journal of *Gastrointestinal Oncology*

World J Gastrointest Oncol 2024 October 15; 16(10): 4037-4299

Published by Baishideng Publishing Group Inc

World Journal of Gastrointestinal Oncology

Contents

Monthly Volume 16 Number 10 October 15, 2024

World Journal of Gastrointestinal Oncology

Monthly Volume 16 Number 10 October 15, 2024

Contents

World Journal of Gastrointestinal Oncology

Monthly Volume 16 Number 10 October 15, 2024

Contents

ABOUT COVER

AIMS AND SCOPE

The primary aim of *World Journal of Gastrointestinal Oncology* (*WJGO*, *World J Gastrointest Oncol*) is to provide scholars and readers from various fields of gastrointestinal oncology with a platform to publish high-quality basic and clinical research articles and communicate their research findings online.

WJGO mainly publishes articles reporting research results and findings obtained in the field of gastrointestinal oncology and covering a wide range of topics including liver cell adenoma, gastric neoplasms, appendiceal neoplasms, biliary tract neoplasms, hepatocellular carcinoma, pancreatic carcinoma, cecal neoplasms, colonic neoplasms, colorectal neoplasms, duodenal neoplasms, esophageal neoplasms, gallbladder neoplasms, *etc*.

INDEXING/ABSTRACTING

The *WJGO* is now abstracted and indexed in PubMed, PubMed Central, Science Citation Index Expanded (SCIE, also known as SciSearch®), Journal Citation Reports/Science Edition, Scopus, Reference Citation Analysis, China Science and Technology Journal Database, and Superstar Journals Database. The 2024 edition of Journal Citation Reports® cites the 2023 journal impact factor (JIF) for *WJGO* as 2.5; JIF without journal self cites: 2.5; 5-year JIF: 2.8; JIF Rank: 71/143 in gastroenterology and hepatology; JIF Quartile: Q2; and 5-year JIF Quartile: Q2. The *WJGO*'s CiteScore for 2023 is 4.2 and Scopus CiteScore rank 2023: Gastroenterology is 80/167; Oncology is 196/404.

RESPONSIBLE EDITORS FOR THIS ISSUE

Production Editor: *Si Zhao*; **Production Department Director:** *Xiang Li*; **Cover Editor:** *Jia-Ru Fan.*

NAME OF JOURNAL
World Journal of Gastrointestinal Oncology

ISSN
ISSN 1948-5204 (online)

LAUNCH DATE
February 15, 2009

FREQUENCY
Monthly

EDITORS-IN-CHIEF
Monjur Ahmed, Florin Burada

EDITORIAL BOARD MEMBERS
https://www.wjgnet.com/1948-5204/editorialboard.htm

PUBLICATION DATE
October 15, 2024

INSTRUCTIONS TO AUTHORS
https://www.wjgnet.com/bpg/gerinfo/204

GUIDELINES FOR ETHICS DOCUMENTS
https://www.wjgnet.com/bpg/GerInfo/287

GUIDELINES FOR NON-NATIVE SPEAKERS OF ENGLISH
https://www.wjgnet.com/bpg/gerinfo/240

PUBLICATION ETHICS
https://www.wjgnet.com/bpg/GerInfo/288

PUBLICATION MISCONDUCT
https://www.wjgnet.com/bpg/gerinfo/208

ARTICLE PROCESSING CHARGE
https://www.wjgnet.com/bpg/gerinfo/242

STEPS FOR SUBMITTING MANUSCRIPTS
https://www.wjgnet.com/bpg/GerInfo/239

ONLINE SUBMISSION
https://www.f6publishing.com

World Journal of Gastrointestinal Oncology

Submit a Manuscript: https://www.f6publishing.com

World J Gastrointest Oncol 2024 October 15; 16(10): 4209-4231

DOI: 10.4251/wjgo.v16.i10.4209

ISSN 1948-5204 (online)

ORIGINAL ARTICLE

Basic Study

Jianpi-Huatan-Huoxue-Anshen formula ameliorates gastrointestinal inflammation and microecological imbalance in chemotherapy-treated mice transplanted with H22 hepatocellular carcinoma

Ya-Nan Wang, Xiang-Yang Zhai, Zheng Wang, Chun-Ling Gao, Sui-Cai Mi, Wen-Li Tang, Xue-Min Fu, Huai-Bang Li, Li-Feng Yue, Peng-Fei Li, Sheng-Yan Xi

Specialty type: Oncology

Provenance and peer review: Unsolicited article; Externally peer reviewed.

Peer-review model: Single blind

Peer-review report's classification

Scientific Quality: Grade A, Grade C, Grade C

Novelty: Grade A, Grade B, Grade C

Creativity or Innovation: Grade A, Grade B, Grade B

Scientific Significance: Grade A, Grade B, Grade B

P-Reviewer: Ricci AD; Rizzo A

Received: April 7, 2024

Revised: August 6, 2024

Accepted: September 3, 2024

Published online: October 15, 2024

Processing time: 172 Days and 5.5 Hours

Ya-Nan Wang, Zheng Wang, Wen-Li Tang, Xue-Min Fu, Huai-Bang Li, Peng-Fei Li, Sheng-Yan Xi, Department of TCM, Xiang'an Hospital, School of Medicine, Xiamen University, Xiamen 361102, Fujian Province, China

Xiang-Yang Zhai, Faculty of Chinese Medicine and State Key Laboratory of Quality Research in Chinese Medicine, Macau University of Science and Technology, Macau 999078, China

Chun-Ling Gao, Department of Radiotherapy, Chenggong Hospital of Xiamen University, PLA 73rd Army Hospital, Xiamen 361003, Fujian Province, China

Sui-Cai Mi, Department of Oncology, Xiamen Hospital of Traditional Chinese Medicine, Xiamen 361015, Fujian Province, China

Li-Feng Yue, Dongzhimen Hospital, Beijing University of Chinese Medicine, Beijing 100700, China

Corresponding author: Sheng-Yan Xi, Doctor, PhD, Associate Chief Physician, Associate Professor, Department of TCM, Xiang'an Hospital, School of Medicine, Xiamen University, No. 4221-122 Xiang'an Nan Road, Xiamen 361102, Fujian Province, China.
xishengyan@xmu.edu.cn

Abstract

BACKGROUND

Jianpi-Huatan-Huoxue-Anshen formula [Tzu-Chi cancer-antagonizing & life-protecting II decoction (TCCL)] is a Chinese medical formula that has been clinically shown to reduce the gastrointestinal side effects of chemotherapy in cancer patients and improve their quality of life. However, its effect and mechanism on the intestinal microecology after chemotherapy are not yet clear.

AIM

To discover the potential mechanisms of TCCL on gastrointestinal inflammation and microecological imbalance in chemotherapy-treated mice transplanted with hepatocellular carcinoma (HCC).

METHODS
Ninety-six mice were inoculated subcutaneously with HCC cells. One week later, the mice received a large dose of 5-fluorouracil by intraperitoneal injection to establish a HCC chemotherapy model. Thirty-six mice were randomly selected before administration, and feces, ileal tissue, and ileal contents were collected from each mouse. The remaining mice were randomized into normal saline, continuous chemotherapy, Yangzheng Xiaoji capsules-treated, and three TCCL-treated groups. After treatment, feces, tumors, liver, spleen, thymus, stomach, jejunum, ileum, and colon tissues, and ileal contents were collected. Morphological changes, serum levels of IL-1β, IL-6, IL-8, IL-10, IL-22, TNF-α, and TGF-β, intestinal SIgA, and protein and mRNA expression of ZO-1, NF-κB, Occludin, MUC-2, Claudin-1, and IκB-α in colon tissues were documented. The effect of TCCL on the abundance and diversity of intestinal flora was analyzed using 16S rDNA sequencing.

RESULTS
TCCL treatment improved thymus and spleen weight, thymus and spleen indexes, and body weight, decreased tumor volumes and tumor tissue cell density, and alleviated injury to gastric, ileal, and colonic mucosal tissues. Among proteins and genes associated with inflammation, IL-10, TGF-β, SIgA, ZO-1, MUC-2, and Occludin were upregulated, whereas NF-κB, IL-1β, IL-6, TNF-α, IL-22, IL-8, and IκB-α were downregulated. Additionally, TCCL increased the proportions of fecal *Actinobacteria*, *AF12*, *Adlercreutzia*, *Clostridium*, *Coriobacteriaceae*, and *Paraprevotella* in the intermediate stage of treatment, decreased the proportions of *Mucipirillum*, *Odoribacter*, *RF32*, *YS2*, and *Rikenellaceae* but increased the proportions of *p_Deferribacteres* and *Lactobacillus* at the end of treatment. Studies on ileal mucosal microbiota showed similar findings. Moreover, TCCL improved community richness, evenness, and the diversity of fecal and ileal mucosal flora.

CONCLUSION
TCCL relieves pathological changes in tumor tissue and chemotherapy-induced gastrointestinal injury, potentially by reducing the release of pro-inflammatory factors to repair the gastrointestinal mucosa, enhancing intestinal barrier function, and maintaining gastrointestinal microecological balance. Hence, TCCL is a very effective adjuvant to chemotherapy.

Key Words: Chinese medicine; Chemotherapy; H22 hepatocellular carcinoma; Intestinal barrier function; Intestinal microecological balance

Core Tip: Jianpi-Huatan-Huoxue-Anshen formula (Tzu-Chi cancer-antagonizing & life-protecting II decoction) down-regulates the NF-κB signaling pathway and the release of inflammatory factors, alleviates intestinal inflammation, improves intestinal morphology, reduces intestinal barrier damage, and maintains the dynamic balance of intestinal microecology. These results reveal the potential role and advantages of Chinese herbal compounds in improving the unbalanced microenvironment after cancer chemotherapy.

Citation: Wang YN, Zhai XY, Wang Z, Gao CL, Mi SC, Tang WL, Fu XM, Li HB, Yue LF, Li PF, Xi SY. Jianpi-Huatan-Huoxue-Anshen formula ameliorates gastrointestinal inflammation and microecological imbalance in chemotherapy-treated mice transplanted with H22 hepatocellular carcinoma. *World J Gastrointest Oncol* 2024; 16(10): 4209-4231
URL: https://www.wjgnet.com/1948-5204/full/v16/i10/4209.htm
DOI: https://dx.doi.org/10.4251/wjgo.v16.i10.4209

INTRODUCTION

Chemotherapy is one of the main treatments for cancer and involves the use of chemotherapeutic drugs to kill cancer cells. However, while chemotherapy inhibits tumor cells, it also produces a series of toxic side effects on normal human tissue. After receiving multiple chemotherapies, patients often experience hematological toxicities such as neutropenia, and gastrointestinal toxicities such as nausea, vomiting, stomatitis, and mucous membrane inflammation. Other side effects include diarrhea, bone marrow suppression, hair loss, phlebitis, organ damage, *etc.*[1,2]. The above-mentioned side effects seriously affect the living pleasure, result in other complications or physical difficulties, and can cause patients to abandon or discontinue treatment.

Recent research has found that the changes and balance in human intestinal microecology are closely related to various diseases and overall health[3,4], and some evidence indicates that intestinal microbes are also closely related to tumor formation[5]. Gastrointestinal damage in patients with cancer is a common toxic side effect induced by chemotherapy. The most common gastrointestinal toxicities are nausea, vomiting, diarrhea, and constipation. Chemotherapy-related diarrhea can cause water and electrolyte disorders, intestinal mucosal damage, intestinal barrier dysfunction, imbalance

of intestinal immune function, intestinal flora imbalance, and intestinal infections[6]. This can ultimately lead to a microecological imbalance of the human gastrointestinal tract and even cause damage to heart and kidney function, worsen the patient's condition, and decrease compliance with treatment, resulting in greater psychological pressure and seriously affecting the therapeutic effect and prognosis.

The intestinal barrier includes epithelial, immune, chemical, and biological barriers, which are not only essential for the nutrient digestion/absorption but also serve as an important barrier against external pathogenic agents or toxins[7]. And epithelial barrier consists of epithelial cells and tight junction (TJ) proteins which include Claudins, ZO-1, Occludin, *etc.* The chemical barrier consists mainly of various mucins and antibacterial proteins, such as MUC-2 and MUC-3. The immune barrier includes various immunoglobulins, with SIgA being the primary one. The biological barrier is made up of various microorganisms. These four barriers work together through various signaling pathways to jointly maintain gastrointestinal microecological balance and physiological stability, thereby protecting human health[8]. Research indicates that NF-κB is an important intracellular protein in the inflammatory response[9,10]. Chemotherapy drugs can stimulate NF-κB protein, leading to an increase in the release of downstream inflammatory proteins such as interleukin (IL)-22 and IL-8. These pro-inflammatory proteins can alter the structure of the four barriers of the digestive tract, reduce the protective role of the gastrointestinal barrier, and disrupt gastrointestinal micro-ecological stability.

Traditional herbal medicine (THM) is widely recognized as an effective therapeutic method for cancer following chemotherapy. Continuous experiments and clinical research have concluded that THM can alleviate the toxic reactions of chemotherapy, reduce psychological pressure, and enhance the comfort of living[11,12]. Jianpi-Huatan-Huoxue-Anshen formula [Tzu-Chi cancer-antagonizing & life-protecting II formula (TCCL)] is a herbal medical compound created by Professor Wang Yan-Hui at Xiamen University. Professor Wang is a renowned Chinese doctor with 40 years of clinical experience in the treatment of cancer patients. The formula is composed of eight different Chinese herbal medicinals: *Codonopsis pilosula* (Codonopsis root; *Dǎng shēn*) 10 g, *Salvia miltiorrhiza Bunge* (Danshen root; *Dān shēn*) 50 g, *Poria cocos* (Schw.) Wolf (poria; *fú líng*) 30 g, *Hordeum vulgare* (Germinated barley; *mài yá*) 20 g, *Ostrea rivularis* Gould (Oyster shell; *Mǔ lì*) 20 g, *Fritillaria usuriensis Maxim.* (Ussuri fritillary bulb; *Píng bèi mǔ*) 30 g, *Citrus reticulata Blanco* (aged tangerine peel; *Chén pí*) 10 g, and *Ziziphus jujuba Mill.* (Spiney date seed; *Suān zǎo rén*) 25 g. Through many years of clinical application, these Chinese medicines have been shown to promote the recovery of gastrointestinal function of patients with cancer after chemotherapy, increase appetite, enhance the immune function, reduce the probability of recurrence, and improve quality of life[13,14].

In the current study, our research group first focused on investigating the effects and possible mechanisms of TCCL on gastrointestinal pathology, intestinal barrier function, and the inflammation-related NF-κB signaling pathway in chemotherapy-treated mice with transplanted hepatocellular carcinoma (HCC). We then examined how TCCL could regulate intestinal microecology.

MATERIALS AND METHODS

Mice and tumor cells

Forty-eight male and 48 female Kunming mice, aged 5 wk and weighing 20 ± 2 g, were provided by Xiamen University Experimental Animal Centre [No. SCXK (Min) 2018-0003 and SYXK (Min) 2018-0009]. The experimental animals were routinely fed and provided with drinking water for one week in a specific pathogen free animal house with a barrier system. The transplanted H22 tumors were from mice with HCC ascites for 1 wk. H22 HCC cell suspension (No. KMCC-001-0527, ≤ 5 passages) was supplied by the Xiamen University Anticancer Research Center.

Experimental drugs

TCCL (Supplementary Table 1) was purchased from the Xiamen Luyan Pharmaceutical Co., Ltd. The active component fingerprinting of TCCL decoction was carried out using the ACQUITY UPLC I-Class ultra-high performance liquid chromatography-quadrupole/orbitrap high resolution mass spectrometry system (Figure 1A and B). The specimens of each herb collected in TCCL were stored in the School of Medicine of Xiamen University for future reference, and were identified and independently verified by Prof. Hong-Juan Bao from Xiamen Medical College. The specimen identification numbers (*Radix Codonopsis*: 170815; *Radix et Rhizoma Salviae Miltiorrhizae*: 170405; *Sclerotium Poriae Cocos*: 170207; *Pericarpium Citri Reticulatae*: 170809; *Bulbus Fritillariae Ussuriensis*: 170516; Fructus Hordei Germinatus: 170704; Semen Ziziphi Spinosae: 170711; *Concha Ostreae*: 170701) were recorded. Yangzhengxiaoji capsules (YZXJ; product number A1711003; national drug approval number Z20040095), containing 0.39 g per capsule and packaged in boxes of 36 capsules, were purchased from Shijiazhuangyiling Pharmaceutical Co., Ltd. An injection of 5-fluorouracil (5-FU, H12020959, product lot number 1707081) containing 250 mg in each 10 mL ampoule, was purchased from Tianjinjinyao Pharmaceutical Co., Ltd. An injection of 0.9% normal saline (H10983065, product number C18050806), was purchased from Jiangxi Kelun Pharmaceutical Co., Ltd.

Medicinal preparation

Pieces of the Chinese herbal decoction TCCL (195 g) were dipped in drinking pure water of 1950 mL for 30 min and decocted. After boiling for 30 min, eight layers of gauze were used to filter the solution. The dregs were then diluted in 1560 mL of distilled water and boiled for another 30 min. After this second boiling, eight layers of gauze were again used for filtration. The two filtrates were combined, filtered through 16 layers of gauze, and concentrated to 120 mL with a rotary evaporator at 58 °C in a water bath. The resulting solution was freeze-dried using a freeze dryer to prepare a lyophilized powder. The lyophilized powder was weighed, and dissolved in distilled water to obtain solutions at final

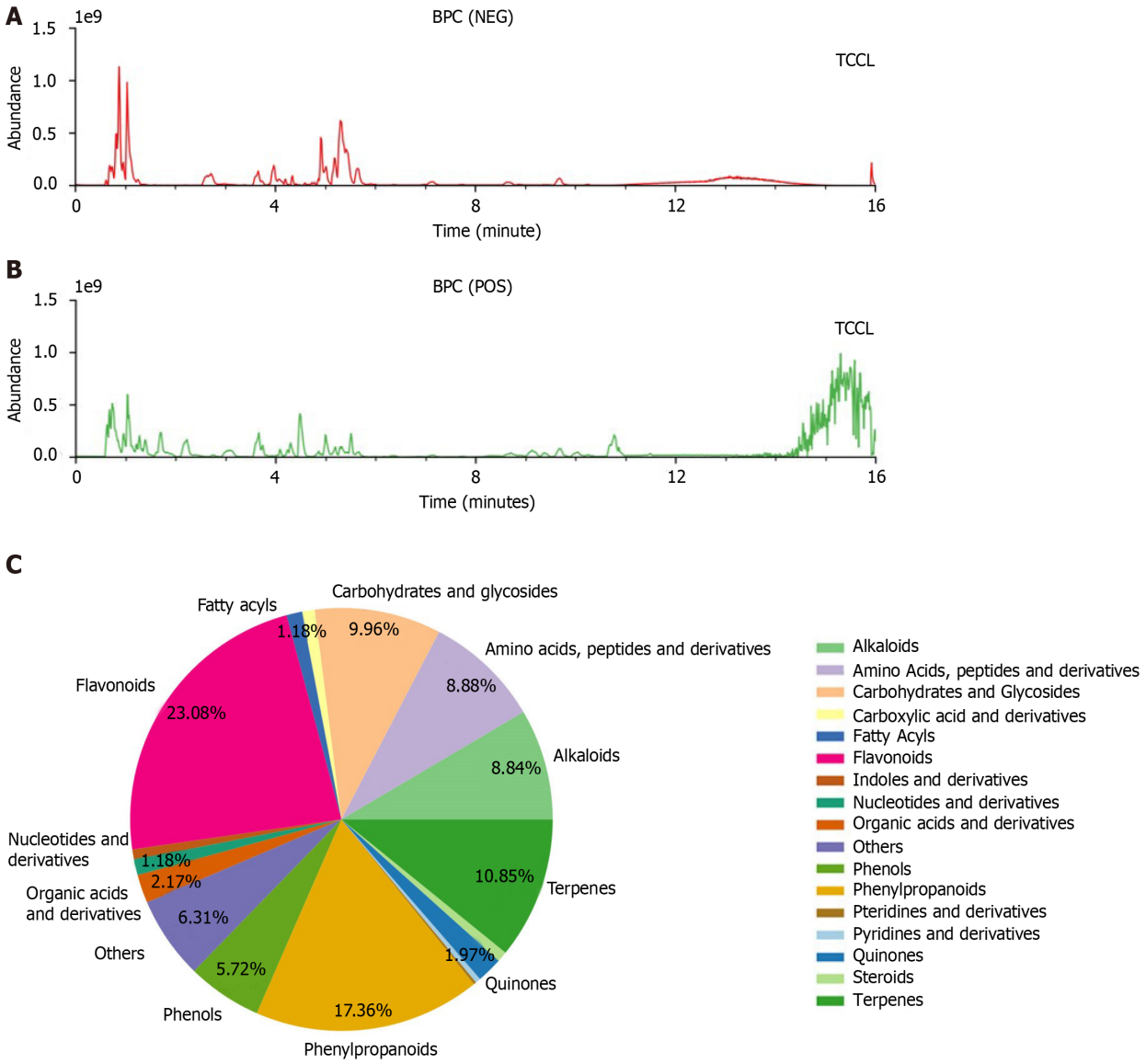

Figure 1 Base peak chromatograms of Tzu-Chi cancer-antagonizing & life-protecting II decoction. A: Negative ion mode; B: Positive ion mode; C: Classification and quantity distribution of Tzu-Chi cancer-antagonizing & life-protecting II decoction components (C). BPC: Base peak chromatogram; TCCL: Tzu-Chi cancer-antagonizing & life-protecting II decoction; NEG: Negative; POS: Positive.

concentrations of 3.24, 1.62, and 0.81 g/mL for intragastric administration (the corresponding dose is 17.6, 8.8, and 4.4 g/kg, about 20, 10, and 5 times the equivalent dose in humans). The YZXJ was dissolved in drinking pure water, and the adjusted concentration was 0.039 g/mL (corresponding to 0.78 g/kg). The 5-FU was diluted to adjust the concentration to 1 mg/mL (corresponding to 20 mg/kg) and 10 mg/mL (200 mg/kg).

Chemotherapy-treated H22 HCC mouse model

Under aseptic conditions, HCC cells from mice with primary H22 hepatic ascites were extracted on an aseptic clean bench (Sujie Clean Equipment Co., Ltd., Suzhou, China). The ascites appeared as a milky white suspension, and the H22 cells were counted under an inverted fluorescence microscope (× 100). H22 cells were labeled with trypan blue, showing that the viability was > 95%, and then diluted with phosphate-buffered saline (PBS) to prepare H22 hepatoma cell suspension. The suspension concentration was adjusted to 2×10^7 cells/mL. A 0.2 mL aliquot (approximately 4×10^6 cells) was inoculated subcutaneously into every mouse's right anterior humerus, creating a small lump at the subcutaneous inoculation site. After the formation of mouse xenografts, a high dose of 5-FU (200 mg/kg, 0.2 mL/10 g) was intraperitoneally injected into each mouse to establish a chemotherapy model of H22 tumor-bearing mice.

Animal groups and drug administration

Before administering the drug, 36 mice were randomly selected from a total of 96 model mice, with six mice per group. Under aseptic conditions, 0.2 g of feces were collected from each mouse. After the mice were humanely euthanized by cervical dislocation, ileal contents (> 500 mg) from the same site were collected and placed in a dry, sterilized centrifuge tube. The samples were then frozen at −80 °C. The remaining 60 mice were randomly assigned into six groups based on

weight and gender: Normal saline (NS control), chemotherapy control (5-FU control), Chinese patent medicine control (Yangzhengxiaoji capsules, YZXJ), and high-, medium-, and low-dose TCCL groups (TCCL-H, TCCL-M, and TCCL-L, with 10 mice per group. Twenty-four hours after modeling, the mice were administered daily doses according to body weight. The NS control group received 0.2 mL/10 g of 0.9% saline intragastrically once daily, while the chemotherapy control group received 25 mg/kg of 5-FU (0.2 mL/10 g) by intraperitoneal injection every 2 d. The Chinese medicine control group received 0.2 mL/10 g of Yangzheng Xiaoji Capsule solution (0.039 g/mL, equivalent to 0.78 g/kg) by gavage once daily. The three TCCL groups received 0.2 mL/10 g of TCCL solution at concentrations of 0.81, 1.62, and 3.24 g/mL TCCL once daily. The treatments were administered continuously for 14 d.

Tumor volume and weight measurement, histology, and calculation of thymus and spleen indexes

Twenty-four hours after the final treatment, the mice were anesthetized with ethyl ether through inhalation and humanely euthanized by cervical dislocation. The long diameter (Ld) and short diameter (Sd) of the transplanted tumor of each mouse were measured. Tumor volume was calculated according to the following formula: V (cm^3) = Ld × Sd × Sd × 1/2. After blood collection from the eyeball, the tumor tissue was dissected and weighed. Tumor, liver, stomach, ileum, and colon tissues were fixed in 10% neutralized formaldehyde solution and cut into paraffin sections (4 μm). Hematoxylin/eosin (H&E)-stained paraffin sections were used for histopathological evaluation, observation, and recording of tissue changes (× 400) with an optical microscope (Olympus Corporation, Tokyo, Japan). The calculation of thymus index and spleen index was performed according to a previous study[15].

Measuring TNF-α, TGF-β, IL-22, IL-1β, IL-8, IL-6, and IL-10 levels in serum, and IgA in jejunal tissue by ELISA

After euthanizing the mice, peripheral blood was collected from the eye using an Eppendorf tube, let stand for 30 min, and centrifuged at 4 °C at 3000 rpm for 15 min. The supernatant was collected. The relevant reagents and samples were stored at 25 °C, equilibrated for 30 min, and then stored until used. Standard and sample wells were prepared separately. One hundred microliters of the standard, the test serum, and the jejunal sample were placed into each well, gently shaken, mixed, and then incubated at 37 °C for 2 h. The liquid was then discarded. Biotin-labeled antibodies (100 μL of TNF-α, IL-22, IL-6, IL-1β, IL-10, IL-8, TGF-β, and SIgA antibodies) were added, and the plate was incubated for 1 h at 37 °C. The liquid was removed, and the plate was dried and washed three times. One hundred microliters of horseradish peroxidase-labeled avidin solution was added into the plates and incubated at 37 °C for 1 h, and the liquid was further discarded. Then the plate was washed 5 times, and 90 μL of the substrate solution was added into the plates, which was then placed at 37 °C for 30 min to allow color to develop. After 50 μL of the stop solution was added to terminate the reaction, the plate was placed in a microplate reader and optical density was read at 450 nm within 15 min. The concentration of each sample was calculated according to the standard curve. The experiments were repeated three times.

Measuring ZO-1, MUC-2, Claudin-1, Occludin, NF-κB, and IκB-α protein expression in colonic tissue by Western blot analysis

Thirty milligrams of colon tissue was homogenized in 200 μL of RIPA lysis buffer for 10 s, incubated for 2 h, and centrifuged at 12000 rpm for 5 min at 4 °C. The supernatant was moved to a new tube and subjected to protein concentration by the BCA method. Equal amounts of proteins were resolved by sodium dodecyl sulfate-polyacrylamide gel electrophoresis and then transferred onto a polyvinylidene fluoride membrane. The membrane was blocked in 5% BSA at 25 °C for 60 min and then incubated with primary antibodies (MUC-2, 1:2000; IκB-α, 1:2000; NF-κB, 1:20000; ZO-1, 1:1000; Occludin, 1:50000; Claudin-1, 1:3000). This was followed by an incubation with an HRP-labeled secondary antibody. Protein bands were then visualized by enhanced chemiluminescencewith enhanced chemiluminescence and quantified with ImageJ software.

Detecting NF-κB, ZO-1, MUC-2, Claudin-1, Occludin, and IκB-α protein expression in colonic tissue by immunohistochemistry

Colonic tissue samples were paraffin-embedded, sectioned, dewaxed, and rehydrated in graded ethanol. Antigen retrieval was then performed by boiling the sections in 0.01 mol/L citric acid buffer at pH 6.0 for 10 min. Endogenous peroxidase activity was then quenched with 3% hydrogen peroxide-methanol. The sections were then blocked with goat serum for 30 min and then incubated with antibodies against ZO-1 (1:500), Occludin (1:200), Claudin-1 (1:100), MUC-2 (1:200), IκB-α (1:100), and NF-κB (1:400) for 15 h at 4 °C, followed by incubation with HRP-labeled goat anti-rabbit/mouse secondary antibody for 20 min at 25 °C. Color was developed with DAB. The sections were subsequently counterstained with hematoxylin for 1 min, mounted with neutral gum, and observed under a light microscope. Granular, brownish-yellow, or brown staining indicated positive protein expression. Each slide was photographed under the microscope and photographs were analyzed with Image-Pro Plus 6.0 software. Six to eight fields of view (× 400) were randomly selected per slide to calculate integrated optical density values.

Measuring ZO-1, MUC-2, Occludin, Claudin-1, IκB-α, and NF-κB gene expression in colonic tissues by real-time PCR

Approximately 80 mg of colonic tissue was used to isolate total RNA with Trizol according to the manufacturer's instructions. After RNA integrity was determined by 1% agarose gel electrophoresis, total RNA was reversed transcribed into cDNA using a cDNA synthesis kit. Thereafter, polymerase chain reaction was conducted using the following primers (designed with Primer Premier 6.0 software): Forward, 5′-GTGCTATGTTGCTCTAGACTTCG-3′ and reverse, 5′-ATGCCACAGGATTCCATACC-3′ for β-actin (174 bp); forward, 5′-AAACCCGAAACTGATGCTGT-3′ and reverse, 5′-CGCCCTTGGAATGTATGTG-3′ for *ZO-1* (151 bp); forward, 5′-GGATCCTGTCTATGCTCATTATTGT-3′ and reverse, 5′-

TTTGGCTGCTCTTGGGTCT-3′ for Occludin (212 bp); forward, 5′-ACAGCATGGTATGGAAACAGAA-3′ and reverse, 5′-GACAGGAGCAGGAAAGTAGGAC-3′ for Claudin-1 (151 bp); forward, 5′-TCTCTATGACCTGGACGACTCTT-3′ and reverse, 5′-GCTCATACGGTTTCCCATTTAGT-3′ for NF-κB (128 bp); forward, 5′-CTCGGAACTCCAGAAAGAAGC-3′ and reverse, 5′-CAGGGAATCGGTAGACATCG-3′ for *MUC-2* (101 bp); and forward, 5′-CTTGGCAATCATCCACGAA-3′ and reverse, 5′-TCACAGGCAAGATGTAGAGGG-3′ for *IκB-α* (222 bp). Amplification parameters were: Pre-denaturation at 95 °C for 10 min, 40 cycles of denaturation at 95 °C for 10 s, annealing at 56 °C for 30 s, and extension at 60 °C for 35 s. β-actin was used as the internal reference, and target gene expression was analyzed using the $2^{-\Delta\Delta CT}$ method.

Measuring abundance and diversity of bacterial species in mouse feces and ileal contents by 16S rDNA sequencing analysis

In addition to the feces and ileal contents collected from 36 mice mentioned above, fecal samples (0.2 g) were collected from 60 mice in each of the remaining six groups on day 7 of administration. On day 14, fecal samples (0.2 g) were again collected from each group under aseptic conditions. After euthanizing the mice, ileal contents (> 500 mg) from the same location were collected, placed in an Eppendorf tube, and stored in a freezer at -80 °C for subsequent analysis. Total DNA was extracted from fecal and ileal contents using the MOBIO (Qiagen) Power Fecal DNA kit. The primers 515F (5′-CCTACGGGNBGCASCAG-3′) and 806R (5′-GGACTACNVGGGTWTCTAAT-3′) were used to amplify the V3-V4 region of the 16S rRNA gene. The amplification procedure was: Pre-denaturation at 95 °C for 180 s, 25 cycles of denaturation at 95 °C for 20 s, annealing at 60 °C for 30 s, and extension at 72 °C for 30 s, and final extension at 72 °C for 10 min. The amplified products were verified by agarose gel (1.5%) electrophoresis and purified with an AxyPrep PCR Cleanup Kit (Axygen Scientific Inc., San Francisco, CA, United States). After the concentration of PCR products was determined by Qubit 3.0, the same concentration of samples were sequenced by Illumina. Purified samples were obtained with the Agilent 2100 Bioanalyser (Agilent Technologies Inc., Clara, CA, United States) and digital real-time PCR was used to detect and quantify the molar concentration of library inserts and libraries, respectively. The libraries that met the requirements were sequenced with an Illumina HiSeq2500 sequencer according to standard procedures.

Statistical analysis

Data are presented as the mean ± SD (or SE) and were analyzed with GraphPad Prism 7.0 software. Statistical difference was determined by both analysis of variance and the Student-Newman-Keuls test. $P < 0.05$ was considered statistically significant.

RESULTS

TCCL components detected by ultra-high performance liquid chromatography-quadrupole/orbitrap high resolution mass spectrometry

Mass spectrograms of TCCL are shown in Figure 1A and B. There were 17 groups of TCCL components obtained by the ultra-high performance liquid chromatography-quadrupole/orbitrap high resolution mass spectrometry (Figure 1C): Flavonoids, fatty acyls, carbohydrates and glycosides, carboxylic acid and derivatives, amino acids, pteridines and derivatives, pyridines and derivatives, alkaloids, terpenes, quinones, steroids, phenylpropanoids, phenols, nucleotides and derivatives, indoles and derivatives, and organic acids and derivatives. The detailed information of 808 active substances determined is shown in Supplementary Table 2.

Effects of TCCL on mouse weight and transplanted tumor weight

Mouse weight and transplanted tumor weight and volume were recorded. As shown in Figure 2, all mice exhibited side effects following chemotherapy, with a significant decrease in body weight (Figure 2A), confirming successful modeling. After 14 d of treatment, except for mouse weight in the 5-FU control group, which continued to decrease, the mouse weight in the other groups increased. Notably, the body weight of mice treated with TCCL returned to the level comparable to that before chemotherapy, with the TCCL-H group showing the most significant increase. In terms of tumor growth, transplanted tumor volume in each group was not obviously different on the 7th day of administration (Figure 2B); however, after 14 d of administration, transplanted tumor volume and mouse weight in the TCCL-H-treated group and 5-FU-treated group were significantly lower than those of the NS-administrated group ($P < 0.05$ or $P < 0.01$; Figure 2C). Moreover, compared with the 5-FU-treated group, transplanted tumor weight/volume in the TCCL-treated groups did not decrease, but tumor growth in TCCL-treated mice obviously slower than that in the NS-administrated group. Compared with mice treated with YZXJ, transplanted tumor weight and volume in mice receiving TCCL-H treatment decreased (Figure 2C and D). These results indicate that TCCL can inhibit tumor growth in the rodent model of H22 HCC after chemotherapy.

Effects of TCCL on thymus and spleen indexes of H22 HCC mice after chemotherapy

As shown in Figure 2E-H, compared to the NS-administrated group, thymus and spleen weight, and thymus & spleen indexes of TCCL-H treated mice were significantly increased ($P < 0.01$; $P < 0.05$), and the spleen index of TCCL-M-treated mice was also significantly increased ($P < 0.01$). Compared with 5-FU-treated mice, thymus and spleen weight, and thymus and spleen indexes of both TCCL-H and TCCL-M-treated mice were significantly increased ($P < 0.01$; $P < 0.05$). Thus, TCCL at appropriate concentrations can protect the immune organs of mice and enhance immune function.

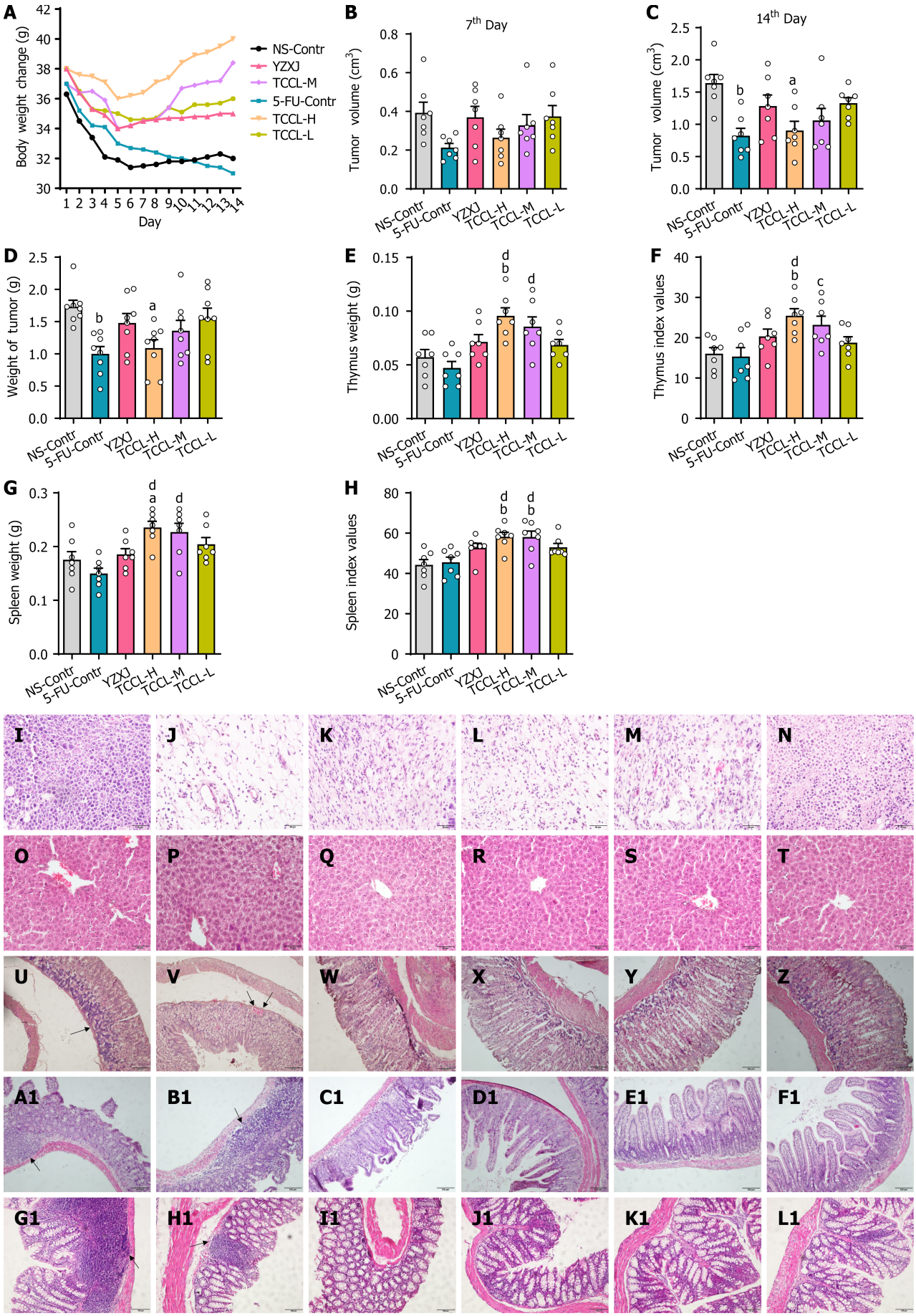

Figure 2 Tzu-Chi cancer-antagonizing & life-protecting II decoction effectively improves body weight, tumor weight/volume, pathological

changes in tumors and the liver, thymus and spleen weight, thymus and spleen indexes, and pathological changes in the stomach, ileum, and colon of H22 hepatocellular carcinoma mice after chemotherapy. Hematoxylin/eosin-stained tissue sections were observed by light microscopy (magnification, × 400). A: Body weight change; B: Tumor volume (7th day); C: Tumor volume (14th day); D-H: Analysis of tumor weight (D), thymus weight (E), thymus index (F), spleen weight (G), and spleen index (H); I-L1: Pathological changes of tumor tissue (I-N), liver tissue (O-T), stomach tissue (U-Z), ileum tissue (A1-F1), and colon tissue (G1-L1) in different groups; I, O, U, A1 and G1: NS-Contr (saline-treated control); J, P, V, B1, and H1: 5-FU-Contr (25 mg/kg); K, Q, W, C1, and I1: Yangzhengxiaoji capsules (0.78 g/kg); L, R, X, D1, and J1: Tzu-Chi cancer-antagonizing & life-protecting II decoction (TCCL)-H (17.6 g/kg); M, S, Y, E1, and K1: TCCL-M (8.8 g/kg); N, T, Z, F1, and L1: TCCL-L (4.4 g/kg). The scale bars for I to T are 50 μm. The scale bars for U to Z and A1 to L1 are 100 μm. Data with error bars are represented as the mean ± SD (n = 6 or 7). [a]P < 0.05 *vs* NS-Contr; [b]P < 0.01 *vs* NS-Contr; [c]P < 0.05 *vs* 5-fluorouracil (FU)-Contr; [d]P < 0.01 *vs* 5-FU-Contr, one-way ANOVA. 5-FU: 5-fluorouracil; YZXJ: Yangzhengxiaoji capsules; TCCL-H: High-dose Tzu-Chi cancer-antagonizing & life-protecting II decoction; TCCL-M: Medium-dose Tzu-Chi cancer-antagonizing & life-protecting II decoction; TCCL-L: Low-dose Tzu-Chi cancer-antagonizing & life-protecting II decoction.

Effects of TCCL on histopathological morphology of H22 tumor, liver, stomach, ileum, and colon tissues

To determine whether TCCL reduces tumor cell growth or attenuates 5-FU-induced gastrointestinal damage, we examined the pathology of tumor, liver, stomach, ileum, and colon tissues by H&E staining and light microscopy at the end of the treatment. As shown in Figure 2I-N, tumor cells in the NS control group were densely packed, with variably sized cells, abnormally enlarged nuclei, and high-grade atypia, as indicated by deep staining. In the 5-FU control group, tumor cells were distributed more loosely, with decreased cell numbers, lighter staining, higher degrees of cell liquefaction, and reduced and ruptured nuclei. In contrast, tumor cells in the TCCL groups exhibited a more loosely arranged pattern with a significant reduction in cell numbers and less atypia compared to the NS control and YZXJ groups. These observations suggest that TCCL has a synergistic inhibitory effect on tumor growth following chemotherapy. As shown in Figure 2O-T, liver structures across all treatment groups appeared nearly normal, with no significant lesions detected. This indicated that TCCL did not cause notable adverse effects on liver tissue in the H22 HCC rodent model after chemotherapy.

As shown in Figure 2U-Z, the gastric mucosal epithelium of mice in the NS control group exhibited significant regional defects with extensive inflammatory cell infiltration. The gastric mucosa of mice in the 5-FU control group showed an incomplete epithelial structure and a few hemorrhagic spots. The YZXJ group displayed mild defects in the gastric mucosal epithelium and minimal inflammatory cell infiltration. In contrast, the TCCL treatment groups demonstrated better structural integrity of the gastric mucosa with minimal inflammatory cell infiltration. These results indicate that TCCL and YZXJ could improve the gastric mucosa following chemotherapy, potentially aiding in the repair or reduction of chemotherapy-induced inflammation. As shown in Figure 2A1-F1 and G1-L1, the ileum and colon of mice in the NS and 5-FU control groups exhibited widespread inflammatory cell infiltration, with notable atrophy and shedding of the ileum villi. The YZXJ group showed ruptured and absent ileum villi. In the TCCL groups, the ileum villi were neatly arranged, and the epithelial structure of the colon remained intact. These findings indicate that TCCL can effectively protect and repair the ileum and colonic mucosa after chemotherapy, reducing the formation and progression of intestinal inflammation.

Effects of TCCL on serum levels of TNF-α, TGF-β, IL-1β, IL-22, IL-6, IL-8, and IL-10 and intestinal SIgA

At the end of the treatment, we measured serum levels of TNF-α, IL-1β, IL-22, IL-6, IL-8, IL-10, and TGF-β and intestinal SIgA content using ELISA. As shown in Figure 3, compared with mice administrated with NS, serum levels of cytokines IL-1β and TNF-α in mice receiving 5-FU treatment were significantly increased (P < 0.01) while IL-10 content was significantly reduced (P < 0.01). In the TCCL-H group, IL-10 and SIgA levels increased significantly (P < 0.01), while the levels of IL-1β, TNF-α, IL-6, IL-8, and IL-22 decreased significantly (P < 0.05 or P < 0.01). The levels of IL-8 and TNF-α after TCCL-M or TCCL-L treatment were reduced (P < 0.05), while the level of TGF-β was enhanced (P < 0.01). The levels of IL-6, TNF-α, and IL-8 after YZXJ treatment were decreased significantly (P < 0.05 or P < 0.01), while the levels of TGF-β and SIgA were increased significantly (P < 0.01). Compared to the 5-FU control group, IL-1β, IL-22, IL-8, IL-6, and TNF-α levels after YZXJ or TCCL treatment were significantly lower (P < 0.05 or P < 0.01), and IL-10 and SIgA levels were significantly increased (P < 0.05 or P < 0.01). And the levels of IL-10, TNF-α, and IL-22 in serum in mice receiving TCCL-H treatment were lower than those in mice treated with YZXJ. These comparisons suggest that TCCL could, to a certain extent, inhibit the expression of pro-inflammatory cytokines and promote the expression of anti-inflammatory cytokines and SIgA.

Effects of TCCL on protein expression levels of colonic ZO-1, NF-κB, Occludin, MUC-2, Claudin-1, and IκB-α

In order to investigate the potential regulatory effect of TCCL on the intestinal barrier, the protein levels of colonic ZO-1, NF-κB, Occludin, MUC-2, and IκB-α in each group of mice were detected. Western blot analysis showed that compared with the NS and 5-FU control groups, the protein levels of ZO-1, MUC-2, and Occludin after TCCL-H or TCCL-M treatment were increased significantly (P < 0.01; Figure 4), whereas the protein levels of colonic NF-κB and IκB-α of the TCCL groups, as well as the protein level of Claudin-1 in the TCCL-H group and IκB-α in the YZXJ group, were significantly reduced (P < 0.05 or P < 0.01; Figure 4). Compared with mice receiving YZXJ treatment, ZO-1 and MUC-2 protein expression was enhanced after TCCL-H or TCCL-M treatment (P < 0.05; Figure 4), and the expression levels of IκB-α in the TCCL-H and TCCL-M groups were reduced significantly (P < 0.05; Figure 4).

As shown in Figure 5, the results of immunohistochemical assays indicated that the protein levels of ZO-1, Occludin, and MUC-2 in the colon tissue of mice receiving TCCL-H treatment were significantly higher compared with those in the NS and 5-FU control groups (P < 0.05 or P < 0.01; Figure 5A, B, and D). The protein levels of Claudin-1, NF-κB, and IκB-α

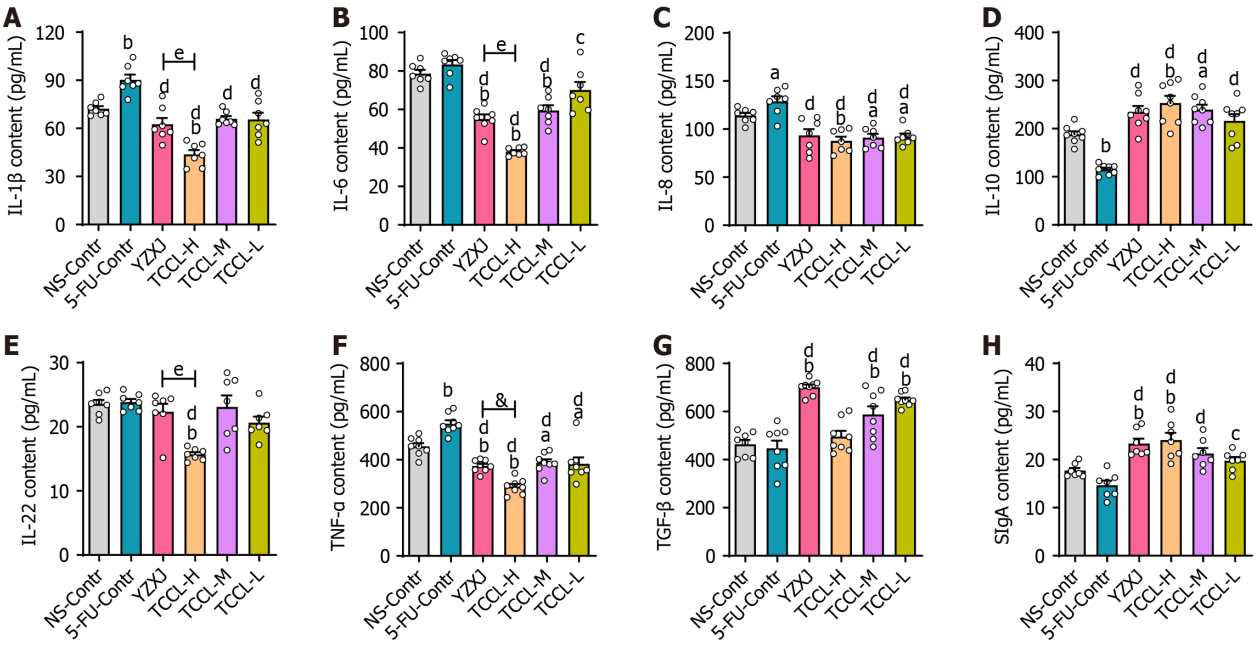

Figure 3 Effects of Tzu-Chi cancer-antagonizing & life-protecting II decoction on serum IL-1β, IL-6, IL-8, IL-22, IL-10, TNF-α, and TGF-β and intestinal SIgA in chemotherapy-treated H22 hepatocellular carcinoma mice. A-G: Contents of serum IL-1β (A), IL-6 (B), IL-8 (C), IL-10 (D), IL-22 (E), TNF-α(F), and TGF-β (G); H: Intestinal SIgA content. Data with error bars are represented as the mean ± SD (n = 6 or 7). $^{a}P < 0.05$ *vs* NS-Contr; $^{b}P < 0.01$ *vs* NS-Contr; $^{c}P < 0.05$ *vs* 5-fluorouracil (FU)-Contr; $^{d}P < 0.01$ *vs* 5-FU-Contr, one-way ANOVA. 5-FU: 5-fluorouracil; YZXJ: Yangzhengxiaoji capsules; TCCL-H: High-dose Tzu-Chi cancer-antagonizing & life-protecting II decoction; TCCL-M: Medium-dose Tzu-Chi cancer-antagonizing & life-protecting II decoction; TCCL-L: Low-dose Tzu-Chi cancer-antagonizing & life-protecting II decoction.

after TCCL-H or TCCL-M treatment were significantly decreased compared with those in mice receiving NS and 5-FU treatment ($P < 0.05$; Figure 5C, E, and F). Compared to mice receiving YZXJ treatment, the protein level of MUC-2 was increased after TCCL-H ($P < 0.05$; Figure 5D). The results of Western blot analysis and immunohistochemistry were basically consistent, suggesting that TCCL could effectively increase the expression levels of both TJ proteins and mucins in intestinal barrier components, reduce the protein expression of inflammatory cytokines, and mitigate the damage to the intestinal mucosa.

Effects of TCCL on mRNA expression levels of colonic ZO-1, Occludin, MUC-2, Claudin-1, NF-κB, and IκB-α

After the mice were treated with TCCL, the mRNA levels of colonic *ZO-1*, *MUC-2*, Claudin-1, *NF-κB*, Occludin, and *IκB-α* were documented as shown in Figure 6. The mRNA levels of *ZO-1*, *MUC-2*, and Occludin after TCCL-H treatment, Occludin after TCCL-M treatment, and MUC-2 after TCCL-L treatment increased significantly compared with those of the NS and 5-FU control groups ($P < 0.05$ or $P < 0.01$). Notably, the *MUC-2* mRNA expression in both the TCCL-H and TCCL-L groups was higher than that in the YZXJ-treated group ($P < 0.05$). *NF-κB* and *IκB-α* mRNA expression levels in the three TCCL groups were decreased significantly compared with those of the NS and 5-FU control groups ($P < 0.05$ or $P < 0.01$). The results of mRNA expression analysis were basically consistent with those of Western blot analysis and immunohistochemistry, indicating that TCCL could effectively protect the main proteins in the intestinal barrier from degradation and inhibit the damage to the mucosal layer of the intestinal wall caused by inflammatory factors.

Effects of TCCL on microbial species in fecal samples and ileal contents in H22 HCC mice receiving chemotherapy

To assess the effect of TCCL on the microflora in feces and ileal contents in mice after chemotherapy, we used 16S rDNA sequencing to analyze fecal samples on day 7 of administration, as well as fecal and ileal content samples before and after day 14. The microbial diversity analysis primarily utilized rarefaction curves to verify whether the amount of data sequenced could reflect the species diversity in feces or ileal contents. In this study, rarefaction curves showed an inflection point at approximately 1000 sequences, with the subsequent curve gradually becoming flatter as sequencing depth increased. When the number of sequences reached 4000, the curves were essentially in the plateau stage, indicating that the amount of sequencing for each sample was sufficient for microbial analysis. Additionally, the Simpson curve of the sample showed an inflection point at 1000 sequences, with the curve gradually flattening thereafter, further demonstrating that the sequencing depth could cover most of the microbes in feces and ileal contents (Supplementary Figure 1).

Alpha diversity analysis

The complexity of microbial community composition in feces and ileal contents was analyzed by α diversity analysis. The α diversity index of each fecal sample and ileal content sample can reflect the microbial community richness (Shannon and Simpson), diversity, and uniformity (ACE, Chao1, and observed species). As shown in Figure 7A-D, in fecal

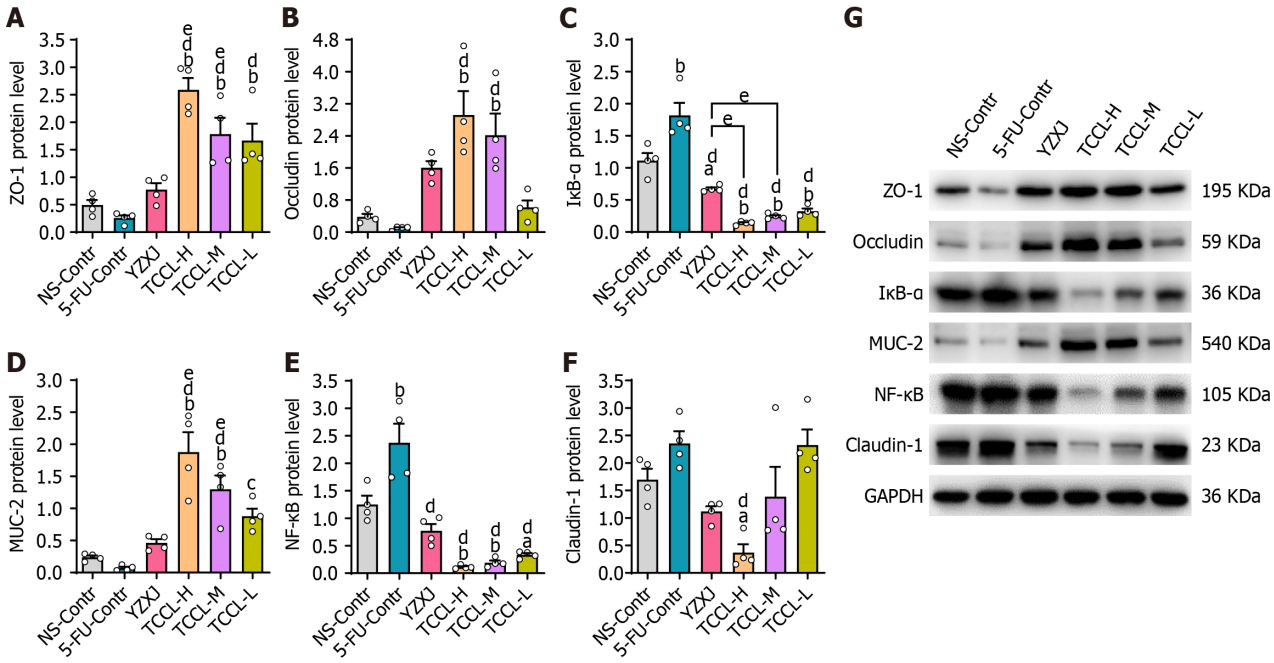

Figure 4 Effects of Tzu-Chi cancer-antagonizing & life-protecting II decoction on protein expression of colonic ZO-1, NF-κB, Occludin, MUC-2, Claudin-1, and IκB-α in H22 hepatocellular carcinoma mice after chemotherapy. A-G: Protein expression of ZO-1 (A), Occludin (B), IκB-α (C), MUC-2 (D), NF-κB (E), and Claudin-1 (F) and band map (G) of each protein by Western blot. Data with error bars are represented as the mean ± SD (n = 4). ^{a}P < 0.05 *vs* NS-Contr; ^{b}P < 0.01 *vs* NS-Contr; ^{c}P < 0.05 *vs* 5-fluorouracil (FU)-Contr; ^{d}P < 0.01 *vs* 5-FU-Contr; ^{e}P < 0.05 *vs* Yangzhengxiaoji capsules, one-way ANOVA. 5-FU: 5-fluorouracil; YZXJ: Yangzhengxiaoji capsules; TCCL-H: High-dose Tzu-Chi cancer-antagonizing & life-protecting II decoction; TCCL-M: Medium-dose Tzu-Chi cancer-antagonizing & life-protecting II decoction; TCCL-L: Low-dose Tzu-Chi cancer-antagonizing & life-protecting II decoction.

specimens, compared with the NS-administrated control group, after 14 d of treatment, the Chao1 and Simpson values in the TCCL-L and YZXJ groups were increased, and the Simpson value was also increased after TCCL-H and TCCL-M treatment (P < 0.05). Compared to pre-treatment results, the Chao1 value in the TCCL-M and TCCL-L groups after 7 d of treatment was enhanced (P < 0.05), and the Shannon value in mice after receiving TCCL-L treatment was enhanced (P < 0.05). Similarly, in the ileal contents after 14 d of treatment, the Chao1 value in the TCCL-L group, ACE values in the TCCL-H and YZXJ groups, and Simpson values in TCCL-H/TCCL-L-treated mice were greater than those in NS-administrated mice (P < 0.05; Figure 7E-H). Moreover, the ACE value in mice after receiving TCCL-H treatment was significantly greater than the pre-treatment value (P < 0.05; Figure 7F). Thus, the α diversity analysis indicated that TCCL could improve the microbial community richness and diversity in mice.

Operational taxonomic unit distribution in fecal samples and ileum contents

After treatment, the total number of operational taxonomic units (OTUs) in feces in the five drug-treated group increased. Except for NS-administrated mice, the number of unique OTUs in the other five groups also increased, indicating that the species diversity in each group increased after treatment. The number of unique OTUs in TCCL-treated mice was obviously lower than that of NS-administrated and 5-FU-treated mice either during or after treatment (Figure 8A and B).

In the ileum contents after treatment, the total number of OTUs was significantly less than that of fecal samples, indicating that the bacterial flora in the ileum and feces was significantly different and there were fewer bacteria in ileum contents than in fecal samples. The number of common OTUs in ileum contents in each group was less than that in mouse fecal samples, but the number of unique OTUs in each group was significantly increased. Specifically, the number of unique OTUs in TCCL-L/TCCL-H-treated mice was obviously greater than that in NS-administrated mice (Figure 8C). The Venn diagram further demonstrated that TCCL treatment significantly affected the microbial community in the rodent intestinal tract.

Analysis of similarities

Analysis of similarities indicated that for the fecal flora in mice, both during and after treatment, the rank of "between" groups was higher than that of other groups, indicating that the difference between the six groups was larger than that within the six groups. There were significant differences between groups (R > 0). The distributions of the fecal flora in the TCCL-H, TCCL-L, and YZXJ groups did not overlap with those of mice receiving NS administration, suggesting that the median values for these four groups were vastly different (P < 0.05). After treatment, the distributions of the fecal flora in TCCL-M, YZXJ, and the NS control groups no longer overlapped, signifying a significant difference in the median values among these three groups (P < 0.05; Figure 8D and E). As for microflora analysis of ileal contents, there were also significant differences among all groups (R > 0). The median values of TCCL-H, TCCL-M, and TCCL-L-treated mice were significantly different from those of mice receiving NS administration (P < 0.05), indicating that the microflora of the three TCCL-treated mice was vastly different (Figure 8F). These results demonstrate that TCCL treatment could significantly

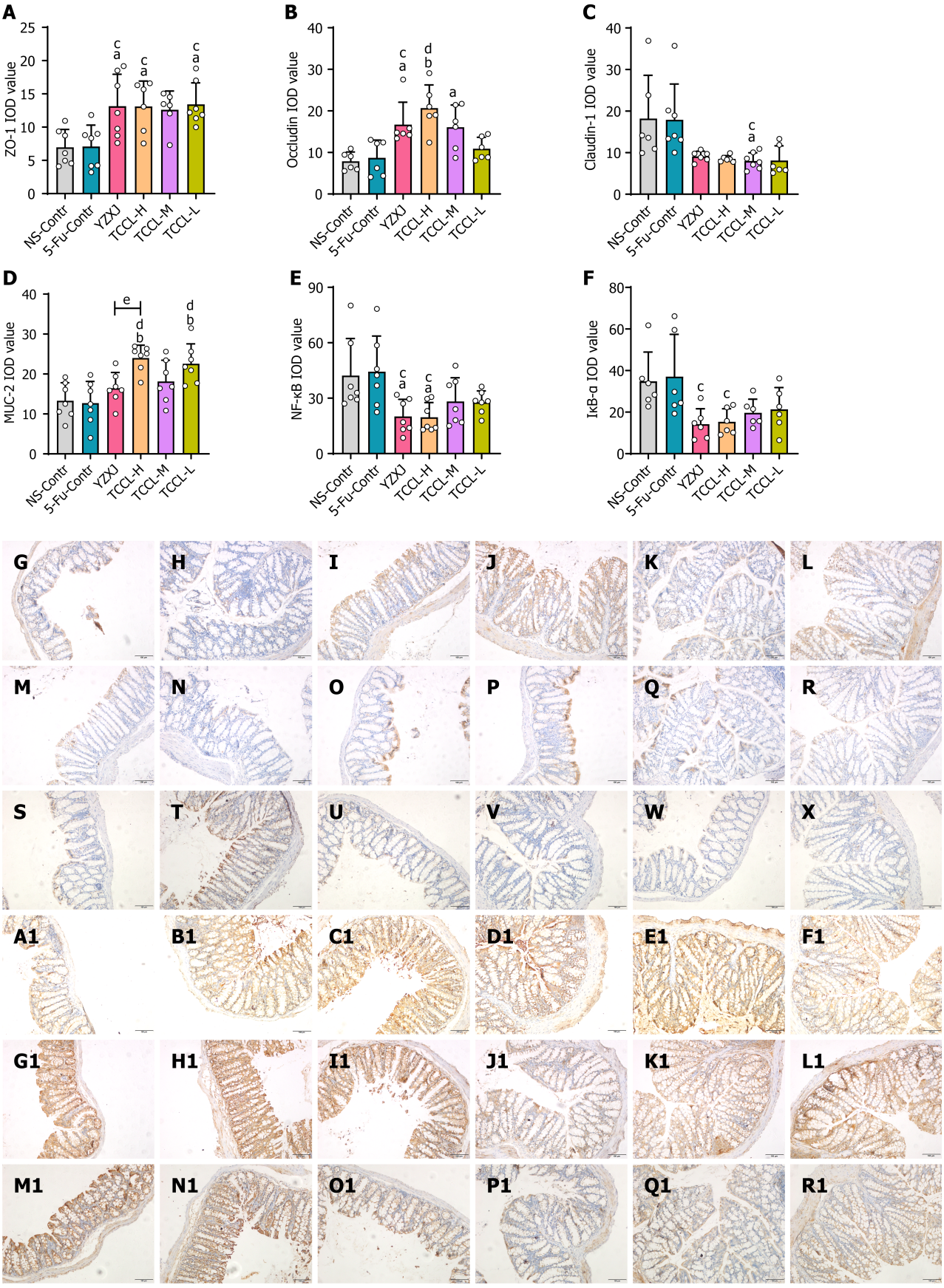

Figure 5 Tzu-Chi cancer-antagonizing & life-protecting II decoction regulates protein expression levels of colonic ZO-1, MUC-2, NF-κB, Occludin, Claudin-1, and IκB-α in H22 hepatocellular carcinoma mice after chemotherapy. A-F: Immunohistochemical analysis of ZO-1 (A), Occludin (B), Claudin-1 (C), MUC-2 (D), NF-κB (E), and IκB-α (F) expression; G-R1: Immunohistochemical images of ZO-1 (G-L), Occludin (M-R), Claudin-1 (S-X), MUC-2 (A1-F1), NF-κB (G1-L1), and IκB-α (M1-R1) in different groups. G, M, S, A1, G1, and M1: NS-Contr (saline-treated control); H, N, T, B1, H1, and N1: 5-

fluorouracil (FU)-Contr (25 mg/kg); I, O, U, C1, I1, and O1: Yangzhengxiaoji (YZXJ) capsules (0.78 g/kg); J, P, V, D1, J1, and P1: Tzu-Chi cancer-antagonizing & life-protecting II decoction (TCCL)-H (17.6 g/kg); K, Q, W, E1, K1 and Q1: TCCL-M (8.8 g/kg); L, R, X, F1, L1 and R1: TCCL-L (4.4 g/kg). The scale bars for G to R1 are 100 μm. Data with error bars are represented as the mean ± SD (n = 6 or 7). [a]P< 0.05 *vs* NS-Contr; [b]P < 0.01 *vs* NS-Contr; [c]P < 0.05 *vs* 5-FU-Contr; [d]P < 0.01 *vs* 5-FU-Contr; [e]P < 0.05 *vs* YZXJ capsules, one-way ANOVA. 5-FU: 5-fluorouracil; YZXJ: Yangzhengxiaoji capsules; TCCL-H: High-dose Tzu-Chi cancer-antagonizing & life-protecting II decoction; TCCL-M: Medium-dose Tzu-Chi cancer-antagonizing & life-protecting II decoction; TCCL-L: Low-dose Tzu-Chi cancer-antagonizing & life-protecting II decoction.

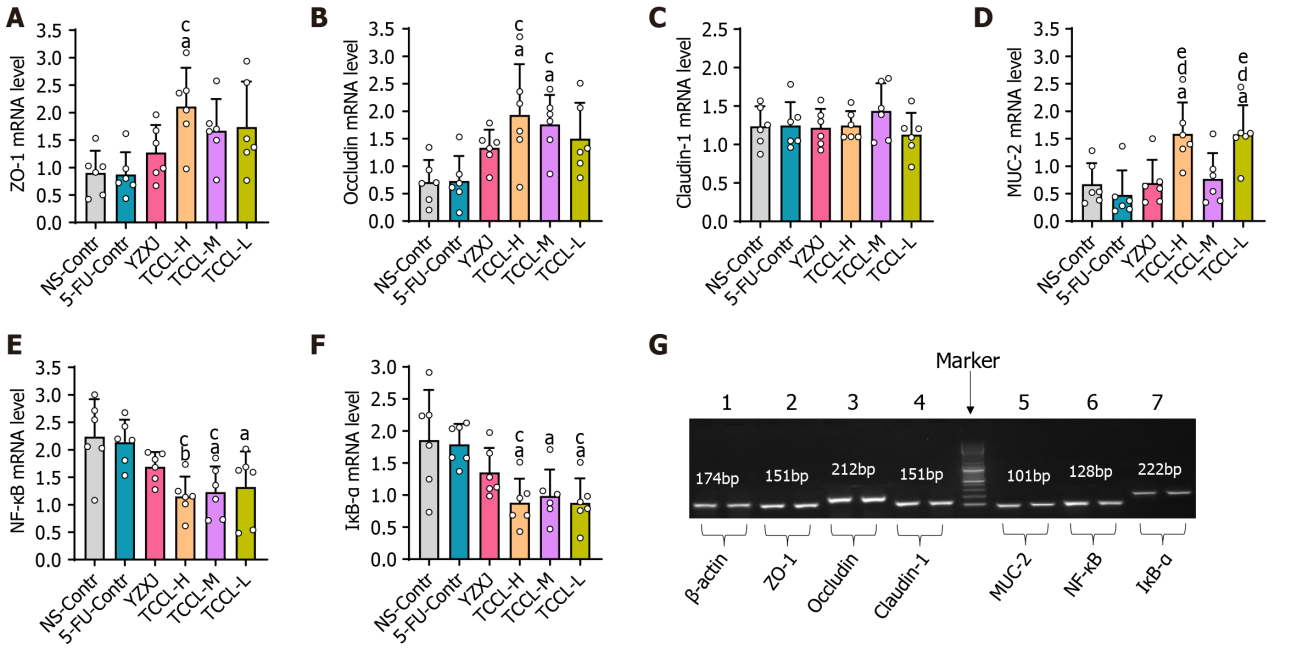

Figure 6 Tzu-Chi cancer-antagonizing & life-protecting II decoction regulates mRNA expression of colonic *ZO-1*, Occludin, Claudin-1, *MUC-2*, *NF-κB*, and *IκB-α* in H22 tumor mice receiving chemotherapy. A-F: The mRNA expression analysis of *ZO-1* (A), Occludin (B), Claudin-1 (C), *MUC-2* (D), *NF-κB* (E), and *IκB-α* (F). G: Gel electrophoretograms of the amplification products of ZO-1, NF-κB, Occludin, Claudin-1, IκB-α, MUC-2, and β-actin obtained after real-time PCR. Data with error bars are represented as the mean ± SD (n = 6). [a]P < 0.05 *vs* NS-Contr; [b]P < 0.01 *vs* NS-Contr; [c]P < 0.05 *vs* 5-fluorouracil (FU)-Contr; [d]P < 0.01 *vs* 5-FU-Contr; [e]P < 0.05 *vs* Yangzhengxiaoji capsules, one-way ANOVA. 5-FU: 5-fluorouracil; YZXJ: Yangzhengxiaoji capsules; TCCL-H: High-dose Tzu-Chi cancer-antagonizing & life-protecting II decoction; TCCL-M: Medium-dose Tzu-Chi cancer-antagonizing & life-protecting II decoction; TCCL-L: Low-dose Tzu-Chi cancer-antagonizing & life-protecting II decoction.

change the species composition of rodent intestinal flora after chemotherapy, distinguishing it markedly from that observed in mice on continuous chemotherapy or without treatment.

Analysis of intestinal flora at phylum and genus levels

Fecal flora analysis in mice revealed that in the pre-treatment and mid-treatment stages, the top three bacteria at the phylum level in the NS control group were *Bacteroidetes*, *Firmicutes*, and *Verrucomicrobia*. The top three bacteria in the TCCL-treated and YZXJ groups were *Firmicutes*, *Bacteroidetes*, and *Proteobacteria* (Figure 9). After treatment, *Bacteroidetes* and *Firmicutes* in the TCCL-treated groups were on the rise compared to those in pre-treatment and mid-treatment stages. The proportion of *Bacteroidetes* in mice receiving TCCL-L treatment decreased, while the proportions of *Bacteroidetes* and *Firmicutes* in mice receiving TCCL-H & TCCL-M treatment were higher than those in the mid-treatment stage. Additionally, the proportions of *Proteobacteria*, *Chlorobacteria*, *Cyanobacteria*, and *p_Deferribacteres* decreased in mice receiving TCCL-H & TCCL-M treatment, whereas the proportion of *Tenericutes* increased slightly (Figure 9). In the further analysis of different bacteria, the number of *Actinobacteria* in mice receiving TCCL-H and TCCL-M treatment was significantly increased compared to that in mice receiving NS administration (P < 0.05) at the phylum level. Compared to mice receiving 5-FU treatment, the number of *Actinobacteria* in mice receiving TCCL-H treatment was significantly increased (P < 0.05; Figure 9L). After treatment, *p_Deferribacteres* in mice receiving TCCL-H treatment were obviously reduced compared with that in mice receiving NS administration, 5-FU, or YZXJ treatment (P < 0.05; Figure 9). In the mid-treatment stage, *AF12*, *Adlercreutzia*, *Clostridium*, and *Coriobacteriaceae* at the genus level increased significantly in mice receiving TCCL-H treatment compared with mice receiving NS administration (P < 0.05 or P < 0.01; Figure 9), and *Paraprevotella* increased significantly in mice receiving TCCL-M treatment (P < 0.05; Figure 9). Compared to mice receiving 5-FU treatment, AF12 in mice receiving TCCL-H treatment was significantly increased (P < 0.05; Figure 9). After treatment, compared to mice receiving NS administration, *Lactobacillus* in mice of the three TCCL-treated groups was significantly increased (P < 0.05 or P < 0.01), while *Mucispirillum*, *Odoribacter*, *Rikenellaceae*, *RF32*, and *YS2* in mice receiving TCCL-H treatment, as well as *YS2* in mice receiving TCCL-M treatment, were significantly decreased (P < 0.05)

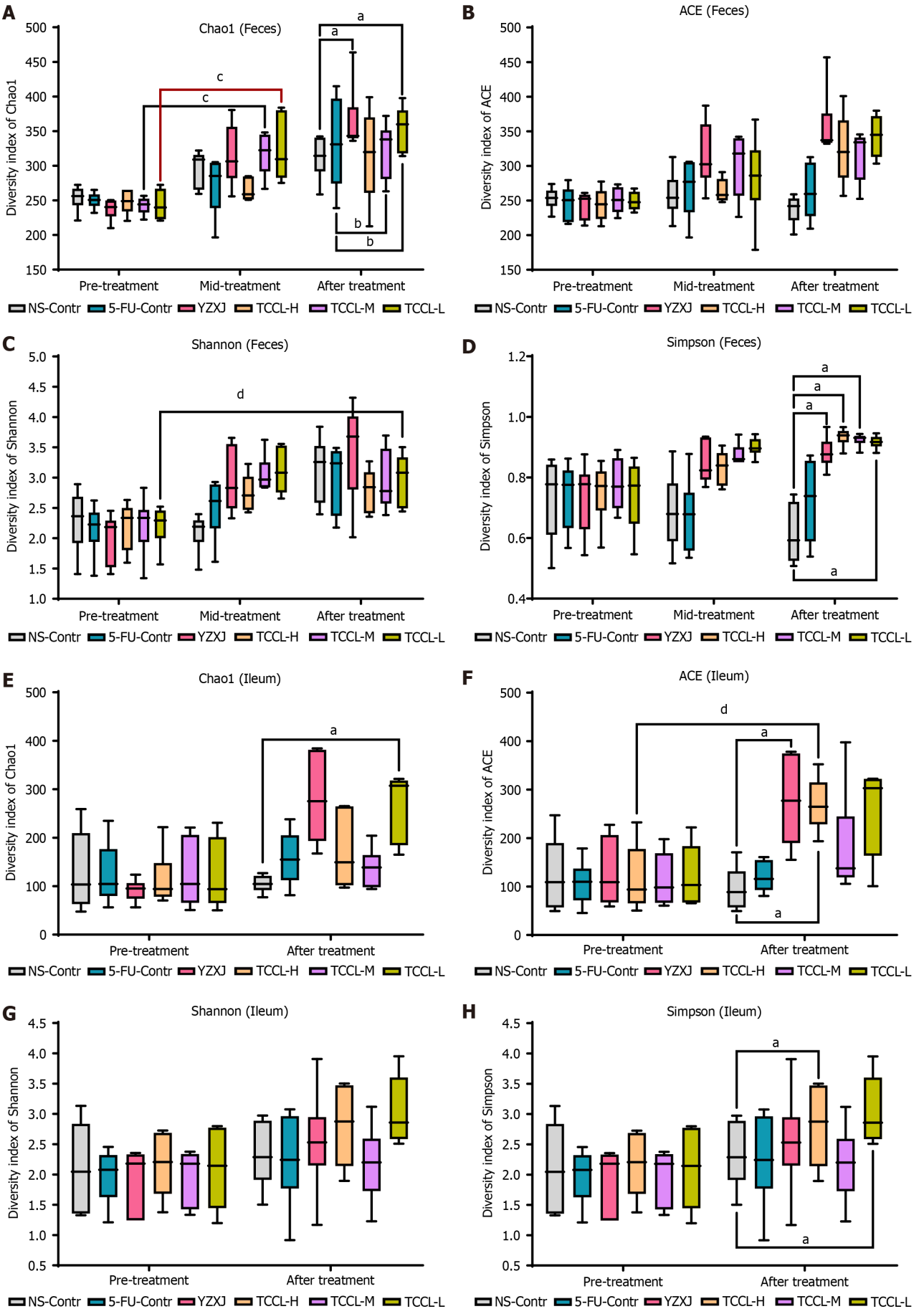

Figure 7 Effects of Tzu-Chi cancer-antagonizing & life-protecting II decoction on microbial community richness, evenness, and diversity

in fecal samples and ileal contents. The horizontal axis represents the groups and the different treatment periods and the vertical axis represents the various alpha indices. A-D: Fecal flora values of Chao1 (A), ACE (B), Shannon (C), and Simpson (D); E-H: Ileum microflora values of Chao1 (E), ACE (F), Shannon (G), and Simpson (H). Data with error bars are represented as the mean ± SD (n = 6). [a]P< 0.05 *vs* NS-Contr; [b]P < 0.05 *vs* 5-fluorouracil-Contr; [c]P < 0.05 pre-treatment *vs* mid-treatment; [d]P < 0.05 pre-treatment *vs* after treatment, one-way ANOVA. 5-FU: 5-fluorouracil; YZXJ: Yangzhengxiaoji capsules; TCCL-H: High-dose Tzu-Chi cancer-antagonizing & life-protecting II decoction; TCCL-M: Medium-dose Tzu-Chi cancer-antagonizing & life-protecting II decoction; TCCL-L: Low-dose Tzu-Chi cancer-antagonizing & life-protecting II decoction.

(Figure 9). Compared with mice receiving 5-FU treatment, *Lactobacillus* in mice receiving TCCL-H treatment was significantly increased (P < 0.05), while *Ruminococcaceae* in mice receiving TCCL-H & TCCL-M treatment and *Mucispirillum* in mice receiving TCCL-H treatment were significantly reduced (P < 0.05; Figure 9).

The analysis of microflora in ileal contents suggested that at the phylum level in the pre-treatment stage and after treatment, the proportion of *Firmicutes* in the ileal contents of mice was significantly higher than that in feces, and the proportion of *Bacteroides* was lower than that in feces, but the two phyla of bacteria were still dominant. However, after treatment, *Verrucomicrobia* and *Proteobacteria* decreased in the three TCCL-treated groups (Figure 10A-D).

Further analysis of differential bacteria in ileal contents showed that after treatment at the genera level, *Lactobacillus*, *Bacteroides*, *Ruminococcus*, and *S24-7* in mice receiving TCCL-H treatment increased significantly compared with mice receiving NS administration (P < 0.05 or P < 0.01; Figure 10); *Mucispirillum* and *Prevotella* were significantly lower (P < 0.05) (Figure 10); and *Lactobacillus* and *S24-7* in mice receiving TCCL-L treatment were significantly increased (P < 0.05; Figure 10). Compared with mice receiving 5-FU treatment, *Lactobacillus* and *S24-7* were significantly increased in mice receiving TCCL-H and TCCL-L treatment (P < 0.01; Figure 10), whereas *Prevotella* was significantly lower (P < 0.05 or P < 0.01; Figure 10).

The analysis of microflora in the ileal contents of mice revealed that, at the phylum level, the proportion of *Firmicutes* in ileal contents after treatment was significantly higher than that in feces, while the proportion of *Bacteroides* was lower than that in feces. Despite these differences, *Firmicutes* and *Bacteroides* remained the dominant phyla. Additionally, after treatment, the proportions of *Verrucomicrobia* and *Proteobacteria* decreased in the three TCCL-treated groups (Figure 10).

Further analysis of differential bacteria in ileal contents showed that after treatment at the genus level, *Lactobacillus*, *Bacteroides*, *Ruminococcus*, and *S24-7* in mice receiving TCCL-H treatment increased significantly compared with mice receiving NS administration (P < 0.05 or P < 0.01; Figure 10); *Mucispirillum* and *Prevotella* were significantly reduced (P < 0.05; Figure 10); and *Lactobacillus* and *S24-7* in mice receiving TCCL-L treatment were significantly increased (P < 0.05; Figure 10). Compared with mice receiving 5-FU treatment, *Lactobacillus* and *S24-7* in mice receiving TCCL-H and TCCL-L treatment were significantly increased (P < 0.01; Figure 10), whereas *Prevotella* was significantly decreased (P < 0.05 or P < 0.01; Figure 10).

Beta diversity analysis

Principal coordinates analysis (PCoA) and non-metric multidimensional scaling (NMDS) are often used to detect the beta diversity of fecal or ileal microbial community. According to the PCoA diagram, the fecal flora of mice during treatment in the NS control group was away from that of the other five treatment groups, indicating marked differences in species composition. Additionally, the distance between the TCCL-H and TCCL-L groups was close, suggesting minimal differences between these two groups of samples (Figure 10). After treatment, compared with feces from mice receiving NS administration, the species composition in feces from mice receiving the other five treatments was significantly different, with minimal variation among samples in the TCCL-L group (Figure 10). In the ileal flora, the species composition in ileal contents from mice receiving TCCL-M and TCCL-L treatment was obviously different from that of mice receiving NS administration, although there was substantial variation within these groups (Figure 10). These results suggest that after TCCL treatment, the microflora in the ileum and feces of mice changed significantly.

NMDS analysis revealed that, whether at mid-treatment or after treatment, the distance between each group receiving drug treatment and the group receiving NS administration was relatively far, and there were obvious differences in the fecal species composition. During mid-treatment, the distances between the TCCL-H and TCCL-L groups and between the TCCL-M and YZXJ groups were small, suggesting minimal differences in microflora between these pairs of groups. After TCCL treatment, the distance between mice receiving TCCL treatment and those receiving NS administration was notably large, reflecting substantial differences in species composition between the groups (Figure 10). In the analysis of microflora in ileal contents, after treatment the distance between the NS control and YZXJ samples was smaller, while the distance between the three TCCL-treated groups and the NS control group was greater. This indicated significant differences in species composition in the TCCL-treated groups compared to the NS control group (Figure 10). The results of the two beta diversity analyses were basically consistent, suggesting that the intestinal flora composition and structure in mice treated with chemotherapy changed significantly after TCCL treatment.

DISCUSSION

Malignant tumors continue to pose a significant health challenge, with their incidence rates rising steadily. Despite some current immunotherapy applications[16-19], effective radical treatments remaining elusive. Thus, identifying improved strategies for cancer management is of great importance. Chemotherapy remains a commonly used approach for treating malignant tumors[20], with the drug 5-FU often employed alone or in combination with other therapies in clinical

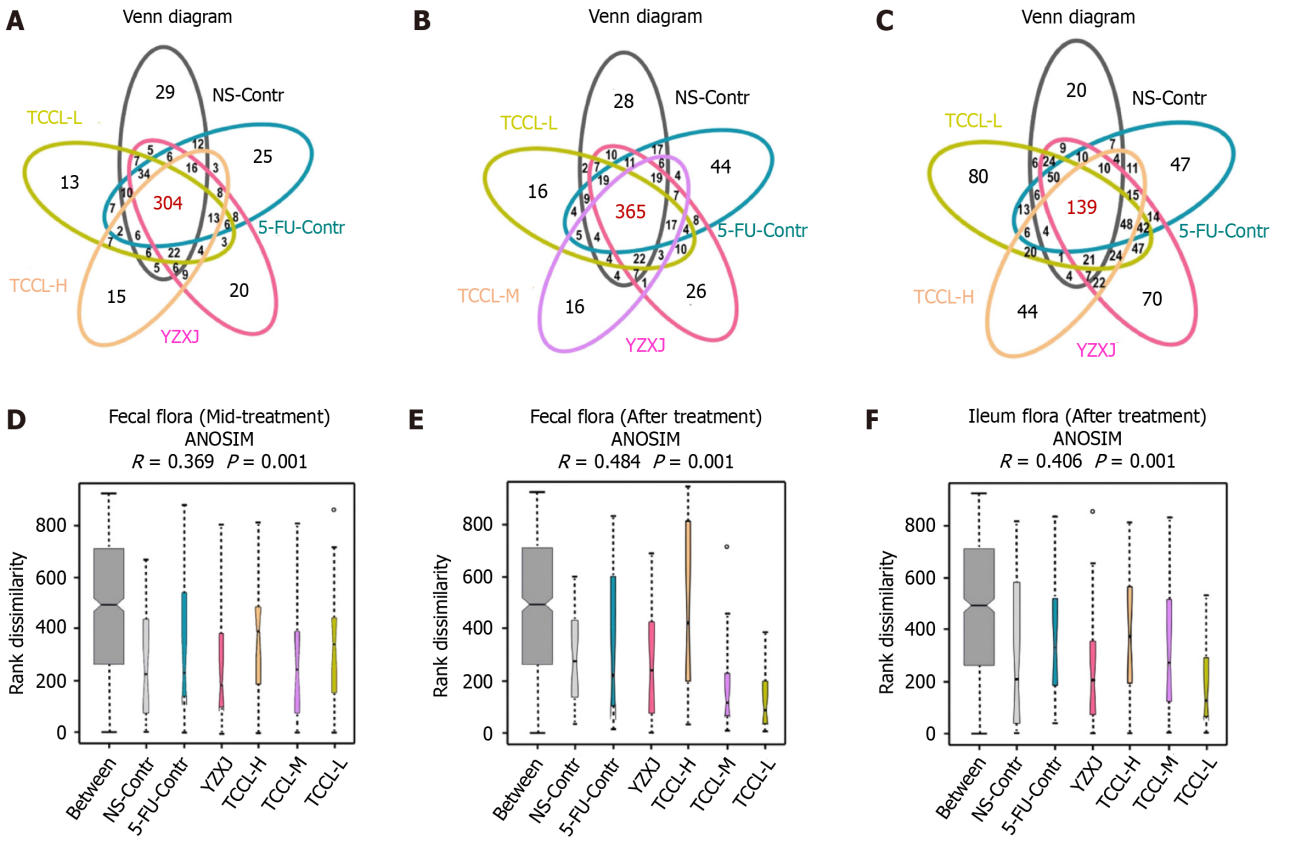

Figure 8 Venn diagrams and analysis of similarities in mid-treatment stage or after Tzu-Chi cancer-antagonizing & life-protecting II decoction treatment. A-C: Venn diagrams of mice feces in the mid-treatment stage (A), mice feces after treatment (B), and mice ileal contents after treatment (C); D-F: Venn diagrams showing the unique and shared operational taxonomic units (OTUs). Different colors indicate different groups, and the number in the middle of the graph represents the number of OTUs. The overlapping areas represent the core microbiome. Analysis of similarities in mice feces in the mid-treatment stage (D), in mice feces after treatment (E), and in mice ileal contents after treatment (F). Data with error bars are represented as the mean ± SD (n = 6 or 7). The x-coordinate represents all samples (between) and each group and the y-coordinate represents the rank of the distance.

settings. Despite its widespread use, 5-FU is associated with issues such as drug resistance and dose-limiting cytotoxicity, which constrain its overall effectiveness in cancer treatment[21]. In clinical practice, patients undergoing multiple rounds of chemotherapy and receiving high doses of 5-FU are often prone to developing intestinal mucositis with severe diarrhea [22], which can lead to decreased appetite, weight loss, and a decline in the quality of life. In our experimental studies, mice with subcutaneously transplanted tumors in the 5-FU chemotherapy group exhibited a continuous decrease in body weight. In contrast, mice in the TCCL-treated groups maintained or returned to normal weight under the same conditions. This suggests that TCCL effectively alleviates intestinal mucosal inflammation induced by 5-FU chemotherapy, improves appetite, and promotes weight gain in mice.

From the perspective of traditional Chinese medicine (TCM), effective cancer management involves maintaining optimal digestive function to ensure that the spleen, stomach, and intestines remain uncompromised, thus sustaining the body's biochemical resources. TCCL, developed by Professor Wang Yan-Hui, a renowned Chinese physician, is based on extensive clinical experience. Clinically, TCCL has been shown to improve gastrointestinal function in patients undergoing tumor chemotherapy, enhance appetite, and boost immune function. It has been experimentally and clinically validated to mitigate the reduction of leukocytes and platelets, reduce pro-inflammatory cell activation, decrease colonic inflammation, promote tumor cell apoptosis, inhibit tumor growth, and enhance patient survival after chemotherapy[13,14]. TCM formulas have been used extensively in cancer treatment and research. YZXJ, a traditional Chinese patent medicine, demonstrates anticancer effects against certain solid tumors. It directly inhibits the adhesion and migration of cancer cells, as well as the angiogenic capabilities of vascular endothelial cells, which may contribute to the suppression of tumor cell growth *in vivo*[23]. In clinical practice, YZXJ has been shown to enhance the quality of life for patients with advanced gastrointestinal cancer by improving appetite, alleviating fatigue, increasing body mass, reducing pain, and enhancing sleep and psychological comfort[24]. It is currently used for treating liver, breast, lung, rectal, and gastric cancers. Consequently, it was chosen as the control drug in this study.

Treatment with 5-FU often induces inflammation in the intestinal mucosal immune system. The intestinal barrier plays a crucial role not only in nutrient digestion and absorption but also as a natural defense against most intestinal pathogens [25]. The intestinal barrier is primarily divided into four components. The first is the epithelial barrier, which consists mainly of intestinal mucosal epithelial cells and TJs. This barrier is crucial for defending against pathogen invasion and plays a significant role in protecting the body from microbial threats. TJs are essential structures that maintain the integrity and permeability of the intestinal mucosal barrier. Cell membrane proteins such as Occludin and Claudin

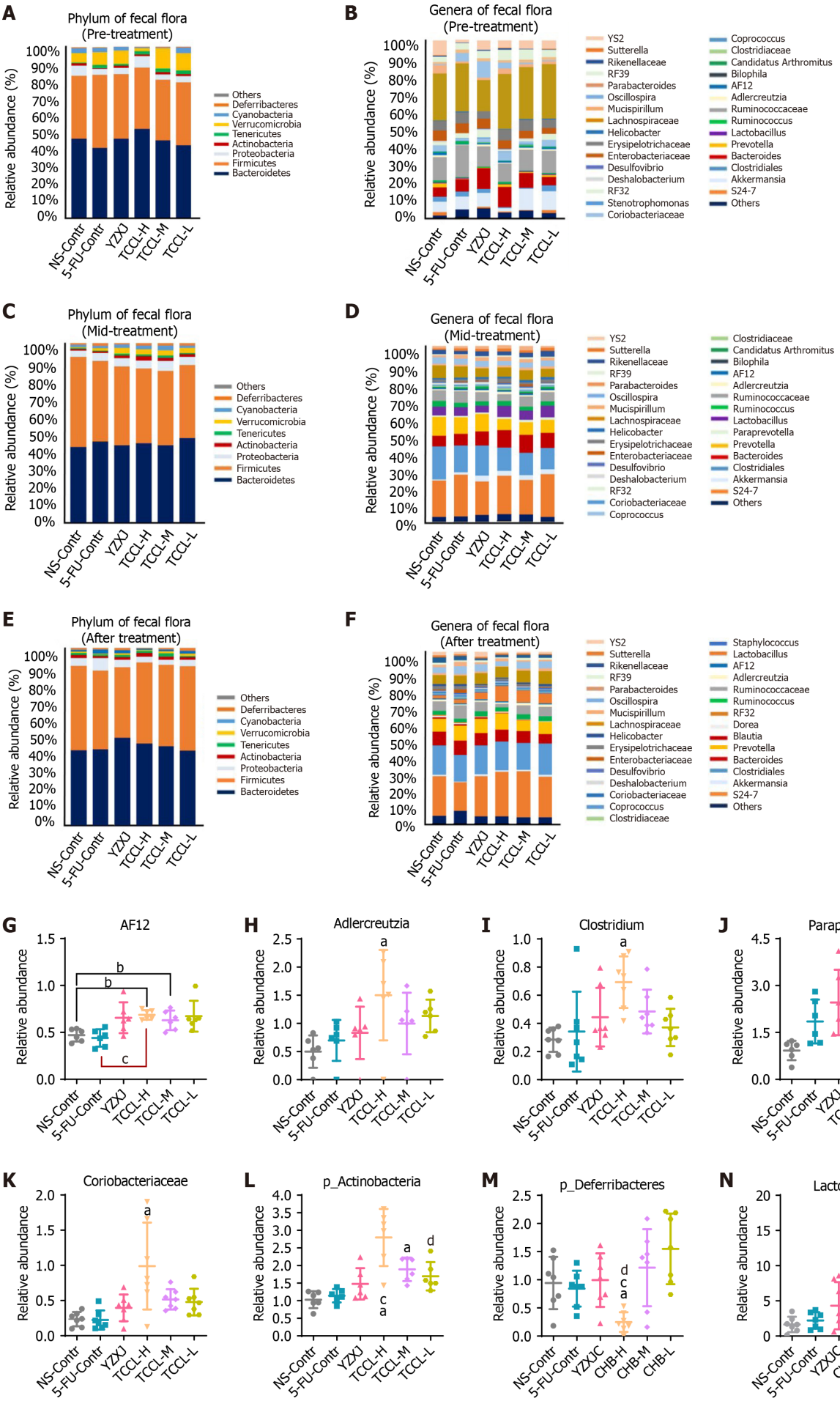
A
Phylum of fecal flora (Pre-treatment)
Relative abundance (%)
Others
Deferribacteres
Cyanobacteria
Verrucomicrobia
Tenericutes
Actinobacteria
Proteobacteria
Firmicutes
Bacteroidetes
NS-Contr
5-FU-Contr
YZXJ
TCCL-H
TCCL-M
TCCL-L
B
Genera of fecal flora (Pre-treatment)
Relative abundance (%)
YS2
Sutterella
Rikenellaceae
RF39
Parabacteroides
Oscillospira
Mucispirillum
Lachnospiraceae
Helicobacter
Erysipelotrichaceae
Enterobacteriaceae
Desulfovibrio
Deshalobacterium
RF32
Stenotrophomonas
Coriobacteriaceae
Coprococcus
Clostridiaceae
Candidatus Arthromitus
Bilophila
AF12
Adlercreutzia
Ruminococcaceae
Ruminococcus
Lactobacillus
Prevotella
Bacteroides
Clostridiales
Akkermansia
S24-7
Others
C
Phylum of fecal flora (Mid-treatment)
D
Genera of fecal flora (Mid-treatment)
Paraprevotella
E
Phylum of fecal flora (After treatment)
F
Genera of fecal flora (After treatment)
Staphylococcus
Blautia
Dorea
G
AF12
H
Adlercreutzia
I
Clostridium
J
Paraprevotella
K
Coriobacteriaceae
L
p_Actinobacteria
M
p_Deferribacteres
N
Lactobacillus
YZXJC
CHB-H
CHB-M
CHB-L

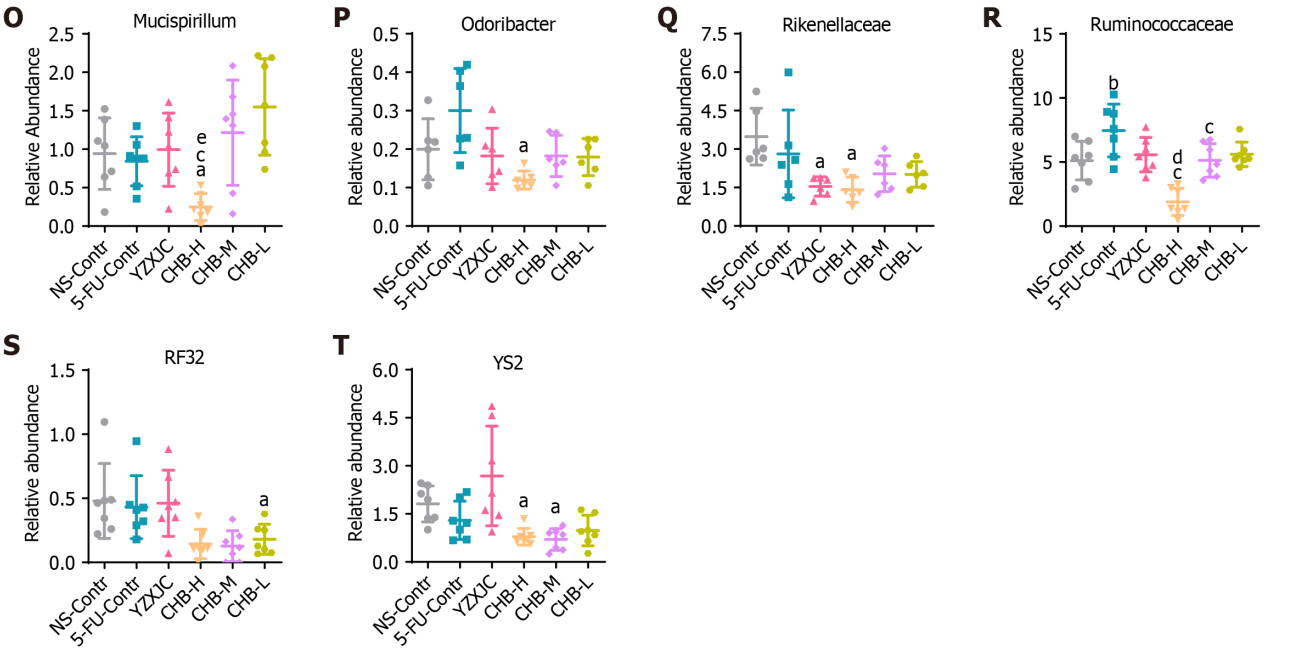

Figure 9 Histograms showing the flora structure of the top eight taxonomic dominant species and the top 30 genus dominant species in fecal samples (with other species having a relative abundance < 1%). A-F: Different microbial species are represented by different colors; the horizontal axis denotes the experimental groups and the vertical axis represents the relative abundance of each species. The histograms highlight the significantly different microbiota between groups in fecal samples during the mid-treatment stage or after treatment. Fecal flora at the phylum level pre-treatment (A), genus level pre-treatment (B), phylum level mid-treatment (C), genus level mid-treatment (D), phylum level after treatment (E), and genus level after treatment (F); G-L: Relative abundance of *AF12* (G), *Adlercreutzia* (H), *Clostridium* (I), *Paraprevotella* (J), *Coriobacteriaceae* (K) and *p_Actinobacteria* (L) in different groups mid-treatment; M-T: Relative abundance of *p_Deferribacteres* (M), *Lactobacillus* (N), *Mucispirillum* (O), *Odoribacter* (P), *Rikenellaceae* (Q), *Ruminococcaceae* (R), *RF32* (S), and *YS2* (T) in different groups after treatment. Data with error bars are represented as the mean ± SD (n = 6 or 7). ^{a}P< 0.05 *vs* NS-Contr; ^{b}P < 0.01 *vs* NS-Contr; ^{c}P < 0.05 *vs* 5-fluorouracil-Contr; ^{e}P < 0.05 *vs* Yangzhengxiaoji capsules, one-way ANOVA. 5-FU: 5-fluorouracil; YZXJ: Yangzhengxiaoji capsules; TCCL-H: High-dose Tzu-Chi cancer-antagonizing & life-protecting II decoction; TCCL-M: Medium-dose Tzu-Chi cancer-antagonizing & life-protecting II decoction; TCCL-L: Low-dose Tzu-Chi cancer-antagonizing & life-protecting II decoction.

proteins, along with cytoplasmic proteins like ZO-1[26], are integral to the barrier and fence functions[27], safeguarding the body from pathogenic microorganisms. When the intestinal TJ barrier is compromised, harmful molecules can infiltrate into deeper layers of the intestine, leading to disturbances and inflammation of the mucosal immune system. This disruption can trigger the development of both intestinal and systemic diseases[28]. The loss of the ZO-1 protein increases permeability before intestinal inflammation develops. Once NF-κB is activated, TNF-α can further increase TJ permeability, thereby reducing ZO-1 protein expression[29] and contributing to intestinal inflammation. In addition to regulating barrier function, members of the Claudin family also control epithelial homeostasis. The downregulation of Claudins-3, 4, 5, 7, 8, and 12 increases the expression of intestinal epithelial Claudins-1, 2, and 18. This alteration in Claudin proteins affects both epithelial and mucosal homeostasis and modifies epithelial barrier function[30]. While the precise role of Occludin remains unclear, numerous studies have highlighted its importance as a structural component of TJs, which regulate the permeability of the epithelial barrier[31,32]. For example, mouse dextran sulfate has been shown to decrease colonic epithelial Occludin protein expression and exacerbate intestinal inflammation[33]. In this study, the expression of ZO-1 and Occludin proteins in mice treated with TCCL was significantly higher compared to that of the NS and 5-FU control groups, while the expression of Claudin-1 protein showed the opposite trend.

The second barrier of the intestine is the chemical barrier, which primarily consists of mucins and antibacterial proteins secreted by intestinal goblet cells and the mucosal epithelium. In sterile mice, the mucus in the small intestine adheres to the epithelium, while the mucus in the colon is permeable, highlighting that the formation of a normal mucus layer depends on the commensal flora[32,34]. The mucus layer features a stable core of the MUC-2 protein, a major glycoprotein in colonic mucus. Deficiency in MUC-2 can impair epithelial barrier function, disrupt intestinal microbiota balance, and lead to spontaneous colitis[35]. MUC-2 is also a principal O-glycosylation product in the small intestine and colon mucus[36]. In this study, the protein expression of MUC-2 was significantly higher in the TCCL-treated groups compared to the NS and 5-FU control groups, indicating that TCCL enhances the expression of MUC-2 protein.

The third barrier of the intestine is the immune barrier, primarily composed of intestinal mucosal lymphoid tissue and SIgA produced by intestinal secretory cells. Lymphoid tissue constitutes about 25% of the gastrointestinal mucosa, utilizing both cellular and humoral immunity to protect the body from pathogenic antigens. SIgA is an acquired immune molecule secreted into the small intestine, playing a crucial role in intestinal immunity. It serves as a key defense mechanism against intestinal toxins and pathogenic microorganisms, safeguarding the intestinal epithelium[37]. Lectins, mucus, and SIgA enhance intestinal mucosal immunity by facilitating the binding of microorganisms to biomolecules, thereby protecting the intestinal barrier function[38]. In this study, the protein expression of SIgA was significantly higher in the TCCL groups compared to the NS control group.

The fourth barrier is the biological barrier. The normal intestinal flora plays a crucial role in colonization resistance against external strains, maintaining the balance of the gastrointestinal microecology and supporting the other three barriers. This collective effort helps protect the intestinal barrier function and preserve the intestinal ecological balance [39]. A healthy gastrointestinal microbial flora requires a certain degree of richness and diversity within the microbial communities in the gastrointestinal tract[40]. The normal microflora in the intestine primarily consists of obligate anaerobic bacteria, such as *Lactobacillus* and *Bifidobacteria*. These probiotics adhere to specific receptors on the surface of the intestinal mucosa, forming a protective membrane structure that shields the body from viruses, bacteria, parasites, fungi, and other pathogens, thus constituting an effective biological barrier. Conversely, dysbiosis of the intestinal flora can lead to various metabolic diseases, such as obesity and diabetes, as well as intestinal inflammatory disorders[41,42]. The results of this study show that the number of *Lactobacillus* was higher in both fecal and ileal flora of mice in the TCCL-H group compared to that of the NS control group.

Chemotherapeutic drugs can destroy the normal intestinal flora, inhibit the growth of probiotics, and disrupt the intestinal biological barrier. This damage indirectly affects other barriers of the intestinal tract, impacting the entire microecological environment. Chemotherapy-induced intestinal inflammation is linked to changes in the intestinal flora, and the use of 5-FU can reduce both the diversity and abundance of this flora. The effects of the intestinal flora and its metabolites on the intestinal mucosa are primarily mediated through the mechanisms described in the following paragraphs[43,44].

First, intestinal bacteria can regulate the activity of pro-inflammatory factors and reactive oxygen species. The intestinal flora and its metabolites can bind to Toll-like receptors on intestinal epithelial cells, activating NF-κB signaling pathways [45]. Activated NF-κB then initiates the production of downstream inflammatory factors, such as IL-6, TNF-α, IL-1β, IL-8, and IL-22[46]. These inflammatory factors can disrupt the epithelial, chemical, and immune barriers of the intestine. Conversely, anti-inflammatory factors such as IL-10 and TGF-β can help mitigate inflammatory responses. Certain probiotics in the intestine, such as *Bifidobacterium* and *Bacteroides polymorphus*, can down-regulate NF-κB expression and inhibit inflammatory responses. *Lactobacillus* and *Bifidobacterium* have been shown to improve 5-FU-induced intestinal mucositis in mice[47]. The secretion of *Clostridium* can inhibit the activation of NF-κB, thereby alleviating local inflammatory reactions. Additionally, *Clostridium* produces short-chain fatty acids, which can significantly reduce colitis in rats and mitigate intestinal adhesion resulting from chemotherapy-induced mucosal microinflammation[48,49]. Studies have found that the colonization of intestinal flora and oxidative reactions within the intestine can influence each other. Chemotherapeutic drugs generate reactive oxygen species, which can damage intestinal epithelial crypt cells, thereby impacting the entire intestinal microbiota[50]. In this study, we found that inflammatory factors such as IL-6, TNF-α, IL-1β, IL-8, and IL-22 were significantly reduced in the TCCL-treated groups compared to the NS control group. Conversely, anti-inflammatory factors like IL-10 and TGF-β were significantly increased. These results suggest that TCCL effectively inhibits the release of inflammatory factors through the NF-κB signaling pathway, thereby reducing intestinal injury and mucosal inflammation.

Second, the intestinal flora and its metabolites can significantly impact intestinal permeability. The epithelial barrier of the intestine is primarily composed of intestinal epithelial cells and the TJs between them. Chemotherapy drugs often lead to atrophy of the intestinal mucosal epithelial villi, which disrupts the mechanical barrier of the intestine, increases permeability, and allows macromolecules such as pathogens and toxins to pass through the gastrointestinal mucosal barrier. This breach can trigger abnormal or secondary immune responses, leading to microbial dysbiosis and potential secondary infections[51]. *Lactobacillus acidophilus* and *Streptococcus thermophilus* can help maintain and enhance the expression of TJ proteins and cytoskeletal proteins in the intestinal epithelial barrier, thereby supporting and preserving intestinal barrier function[52]. In this study, pathological analysis revealed that the mucosal epithelium of the stomach, ileum, and colon tissues in the NS and 5-FU control groups exhibited significant damage, including villous atrophy and shedding. In contrast, the mucosal condition of the mice treated with TCCL was notably improved. These findings suggest that TCCL effectively mitigates the increase in intestinal permeability caused by chemotherapy drugs and reduces damage to the intestinal mucosa. The repair of intestinal mucosal damage appears to be closely linked to the inhibition of inflammatory factor release and the regulation of bacterial community composition and richness.

Third, the intestinal flora influences the composition of the intestinal mucous layer. Chemotherapy drugs can inhibit the proliferation of crypt cells in the intestinal epithelium, thereby disrupting the normal function of the intestinal lining. MUC-2 and MUC-3 are crucial for maintaining the stability of the intestinal mucous layer. It has been confirmed that certain Lactobacilli, such as *Lactobacillus rhamnosus* and *Lactobacillus acidophilus*, as well as nicotinic acid produced by some intestinal bacteria, can upregulate MUC-2 and MUC-3 expression, thereby increasing intestinal mucus secretion [53]. In this study, the increase in *Lactobacillus* led to higher secretion of niacin, which, in turn, significantly elevated the expression level of MUC-2 in the TCCL-H and TCCL-M groups compared to other groups, particularly the NS and 5-FU control groups. This enhancement helped protect the normal function of the intestinal mucous layer.

Finally, the intestinal flora can influence the release of intestinal immune factors. SIgA plays a crucial role in intestinal immunity; as the first line of defense in the intestinal mucosa, it not only protects against foreign invasions and pathogenic bacteria but also promotes the growth and propagation of beneficial bacteria while eliminating harmful ones [49]. Glutamine supplementation can enhance intestinal SIgA secretion in mice through the intestinal microbiome[54]. The experimental results revealed that SIgA secretion in the jejunum of mice in the TCCL treatment group was significantly higher than that in the NS and 5-FU control groups. This increase in SIgA may be related to the growth and proliferation of certain probiotics in the intestine, with elevated SIgA levels potentially further promoting the proliferation of these beneficial bacteria.

Although this study provides a comprehensive analysis of TCCL's role in gastrointestinal microecology from an experimental perspective (Figure 11), several aspects remain to be clarified. The active components of TCCL have not been fully elucidated, some chemical components remain undetermined, and their specific roles and interactions with the

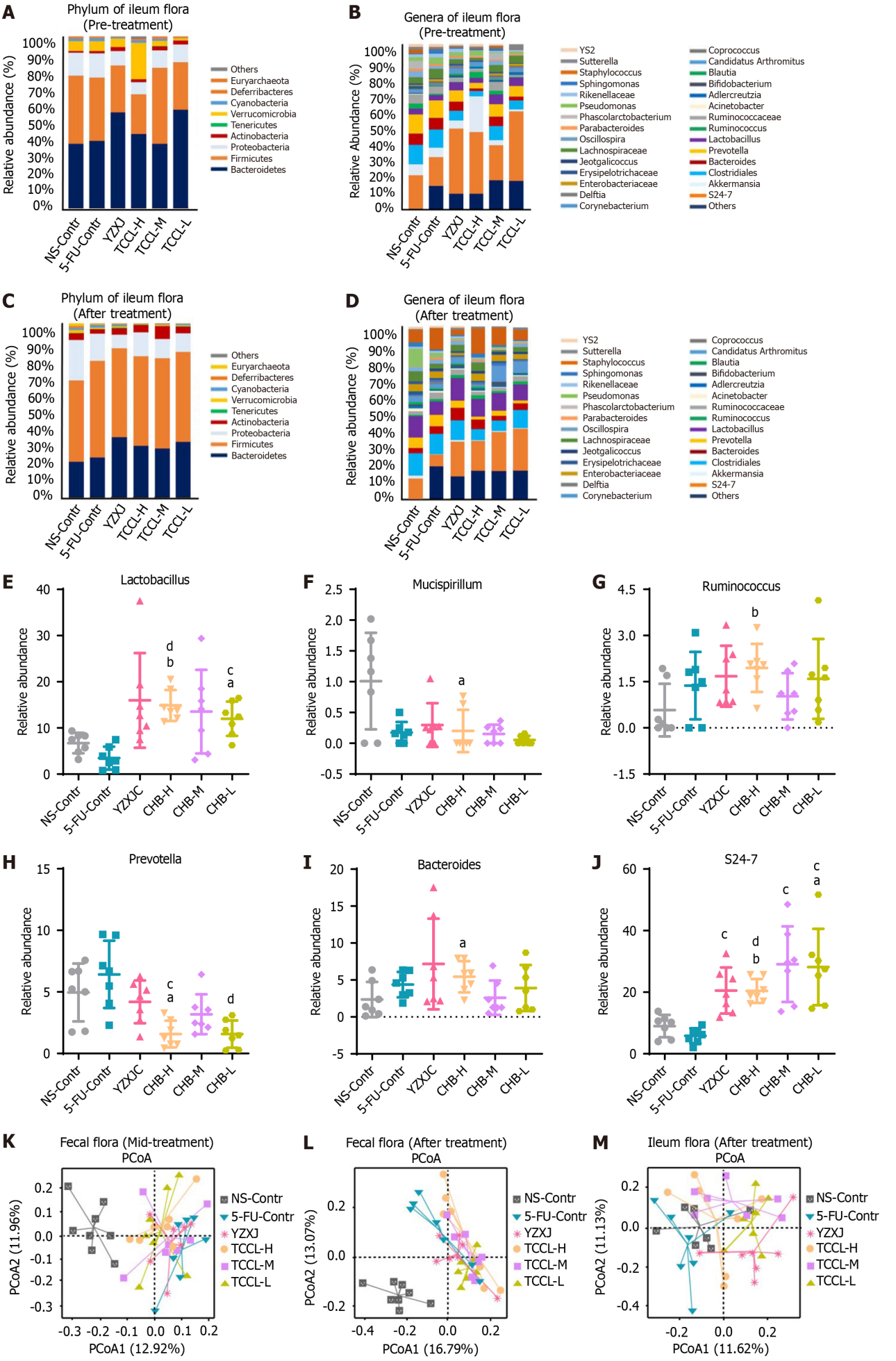
A
Phylum of ileum flora (Pre-treatment)
Relative abundance (%)
Others
Euryarchaeota
Deferribacteres
Cyanobacteria
Verrucomicrobia
Tenericutes
Actinobacteria
Proteobacteria
Firmicutes
Bacteroidetes
NS-Contr
5-FU-Contr
YZXJ
TCCL-H
TCCL-M
TCCL-L
B
Genera of ileum flora (Pre-treatment)
Relative Abundance (%)
YS2
Sutterella
Staphylococcus
Sphingomonas
Rikenellaceae
Pseudomonas
Phascolarctobacterium
Parabacteroides
Oscillospira
Lachnospiraceae
Jeotgalicoccus
Erysipelotrichaceae
Enterobacteriaceae
Delftia
Corynebacterium
Coprococcus
Candidatus Arthromitus
Blautia
Bifidobacterium
Adlercreutzia
Acinetobacter
Ruminococcaceae
Ruminococcus
Lactobacillus
Prevotella
Bacteroides
Clostridiales
Akkermansia
S24-7
Others
C
Phylum of ileum flora (After treatment)
D
Genera of ileum flora (After treatment)
E
Lactobacillus
Relative abundance
NS-Contr
5-FU-Contr
YZXJC
CHB-H
CHB-M
CHB-L
F
Mucispirillum
G
Ruminococcus
H
Prevotella
I
Bacteroides
J
S24-7
K
Fecal flora (Mid-treatment)
PCoA
PCoA2 (11.96%)
PCoA1 (12.92%)
L
Fecal flora (After treatment)
PCoA2 (13.07%)
PCoA1 (16.79%)
M
Ileum flora (After treatment)
PCoA2 (11.13%)
PCoA1 (11.62%)

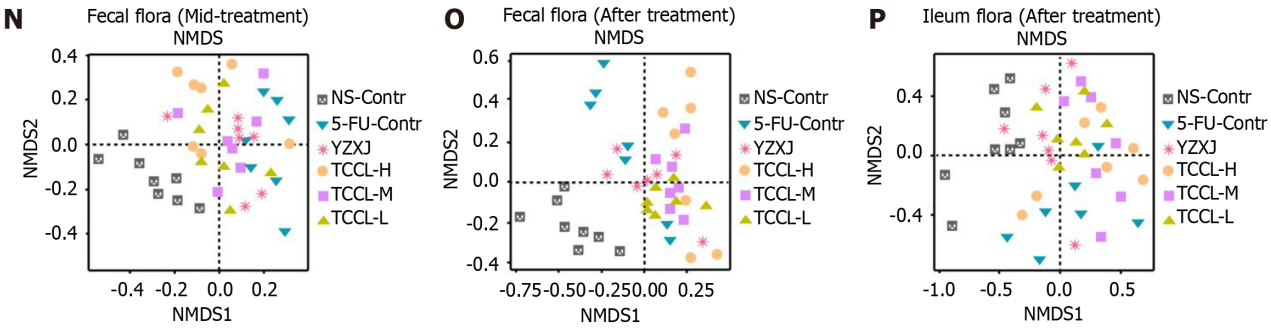

Figure 10 Histograms illustrating the flora structure of the top eight taxonomic dominant species and the top 30 genus dominant species in ileal contents. Species with a relative abundance < 1% are categorized as "others," and different microbial species are represented by distinct colors. The histograms highlight the significantly different microbiota in ileal contents between groups after treatment. Additionally, principal coordinates analysis (PCoA) and nonmetric multidimensional scaling (NMDS) analyses of microflora in both feces and ileal contents are presented. Each point in these analyses represents a sample, with different colors indicating different experimental groups. A-D: Flora in ileal contents at the phylum level before treatment (A), genus level before treatment (B), phylum level after treatment (C), and genus level after treatment (D); E-J: Relative abundance of *Lactobacillus* (E), *Mucispirillum* (F), *Prevotella* (G), *Bacteroides* (H), *Ruminococcus* (I), and *S24-7* (J) in different groups after treatment; K and L: Scatter plots of PCoA analysis results of fecal flora in the mid-treatment stage (K) and after treatment (L). M: Scatter plot of PCoA analysis results of ileal contents after treatment; N and O: Scatter plots of NMDS analysis results of fecal flora in the mid-treatment stage (N) and after treatment (O); P: Scatter plot of NMDS analysis results of ileal contents after treatment. Data with error bars are represented as the mean ± SD (n = 7 or 8). ^{a}P< 0.05 *vs* NS-Contr; ^{b}P < 0.01 *vs* NS-Contr; ^{c}P < 0.05 *vs* 5-fluorouracil (FU)-Contr; ^{d}P < 0.01 *vs* 5-FU-Contr, one-way ANOVA. 5-FU: 5-fluorouracil; YZXJ: Yangzhengxiaoji capsules; TCCL-H: High-dose Tzu-Chi cancer-antagonizing & life-protecting II decoction; TCCL-M: Medium-dose Tzu-Chi cancer-antagonizing & life-protecting II decoction; TCCL-L: Low-dose Tzu-Chi cancer-antagonizing & life-protecting II decoction; PCoA: Principal coordinates analysis; NMDS: Nonmetric multidimensional scaling.

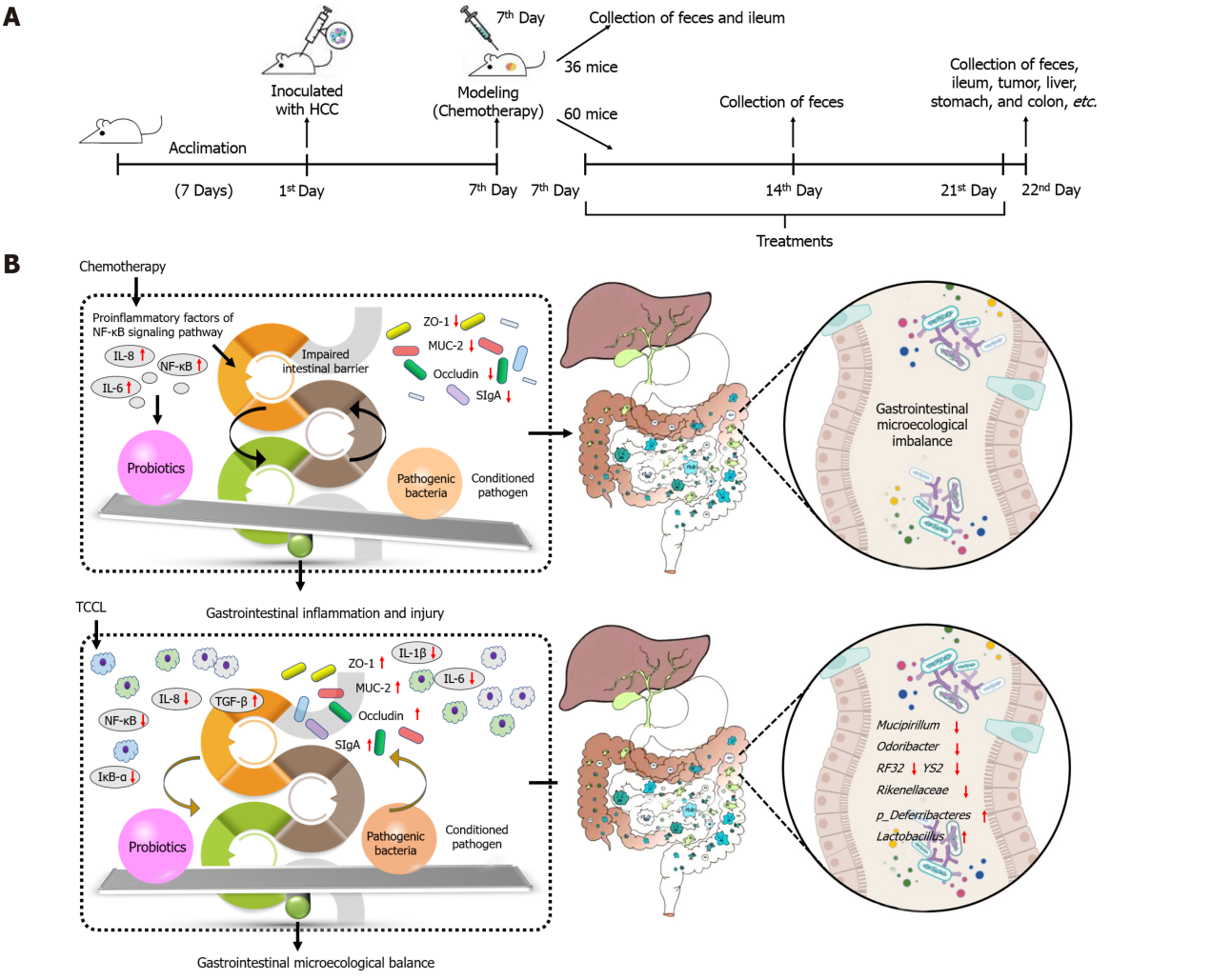

Figure 11 Experimental flow chart and graphical abstract. A and B: Experimental flow chart (A) and graphical abstract (B) of Tzu-Chi cancer-antagonizing

& life-protecting II decoction ameliorating gastrointestinal inflammation and microecology in chemotherapy-treated mice transplanted with H22 hepatocellular carcinoma. TCCL: Tzu-Chi cancer-antagonizing & life-protecting II decoction; HCC: Hepatocellular carcinoma.

microbiota need further investigation. Additionally, the effects of TCCL in other tumor chemotherapy models warrant further exploration.

CONCLUSION

The current study is the first to report that TCCL is effective in regulation of microecology of the gastrointestinal tract in chemotherapy-treated mice with H22 tumors. The potential possible mechanism may be related to its down-regulation of the NF-κB pathway and the release of inflammatory factors, therefore alleviating intestinal inflammation, improving intestinal morphology, reducing intestinal barrier damage, and maintaining the dynamic balance of intestinal microecology. Together, these results suggest that TCCL is a promising adjuvant to chemotherapy.

ACKNOWLEDGEMENTS

We are grateful to Professor Yue-Wen Gong at the University of Manitoba for his efforts in revising the language of this article.

FOOTNOTES

Author contributions: Wang YN was responsible for methodology, data curation, and writing of the original draft; Zhai XY was responsible for methodology and validation; Wang Z was responsible for methodology and data curation; Gao CL, Mi CS, Tang WL, Fu XM, and Li HB were responsible for methodology; Yue LF was responsible for manuscript review & editing; Li PF was responsible for project administration; Xi SY was responsible for manuscript review & editing, funding acquisition, supervision, and project administration; all authors have read and agreed to the published version of the manuscript.

Supported by Natural Science Foundation of Xiamen, China, No. 3502Z20227171; the Young Investigator Research Program of Xiang'an Hospital of Xiamen University, No. XAH23005; the Traditional Chinese Medicine Foundation of Xiamen, No. XWZY-2023-0103; Natural Science Foundation of Fujian, China, No. 2018J01136; and National Natural Science Foundation of China, No. 81202659.

Institutional animal care and use committee statement: All experimental steps of this experiment have been approved by the Animal Management Ethics Committee of Xiamen University (XMULAC-20170018).

Conflict-of-interest statement: The authors declare that there are no known competing financial interests or personal relationships among all authors of this article that could influence all studies reported in this article.

Data sharing statement: The data of this study are available from the corresponding author or any co-author on request.

ARRIVE guidelines statement: The authors have read the ARRIVE guidelines, and the manuscript was prepared and revised according to the ARRIVE guidelines.

Country of origin: China

ORCID number: Chun-Ling Gao 0000-0003-1720-9890; Sui-Cai Mi 0000-0002-1378-9915; Sheng-Yan Xi 0000-0002-8315-6742.

Corresponding Author's Membership in Professional Societies: China Association for Research and Advancement of Chinese Traditional Medicine, CRACM-CCXX-01-016.

S-Editor: Lin C
L-Editor: Wang TQ
P-Editor: Zhao S

REFERENCES

1 **Hauner K**, Maisch P, Retz M. [Side effects of chemotherapy]. *Urologe A* 2017; **56**: 472-479 [PMID: 28251254 DOI: 10.1007/s00120-017-0338-z]

2 **Smita P**, Narayan PA, J K, Gaurav P. Therapeutic drug monitoring for cytotoxic anticancer drugs: Principles and evidence-based practices. *Front Oncol* 2022; **12**: 1015200 [PMID: 36568145 DOI: 10.3389/fonc.2022.1015200]

3 **Jung JY**, Ahn Y, Khare S, Gokulan K, Piñeiro SA, Cerniglia CE. An in vitro study to assess the impact of tetracycline on the human intestinal microbiome. *Anaerobe* 2018; **49**: 85-94 [PMID: 29294359 DOI: 10.1016/j.anaerobe.2017.12.011]

4 **Gomaa EZ**. Human gut microbiota/microbiome in health and diseases: a review. *Antonie Van Leeuwenhoek* 2020; **113**: 2019-2040 [PMID: 33136284 DOI: 10.1007/s10482-020-01474-7]

5 **Hrncir T**, Hrncirova L, Kverka M, Tlaskalova-Hogenova H. The role of gut microbiota in intestinal and liver diseases. *Lab Anim* 2019; **53**: 271-280 [PMID: 30580671 DOI: 10.1177/0023677218818605]

6 **McQuade RM**, Stojanovska V, Abalo R, Bornstein JC, Nurgali K. Chemotherapy-Induced Constipation and Diarrhea: Pathophysiology, Current and Emerging Treatments. *Front Pharmacol* 2016; **7**: 414 [PMID: 27857691 DOI: 10.3389/fphar.2016.00414]

7 **Salvo Romero E**, Alonso Cotoner C, Pardo Camacho C, Casado Bedmar M, Vicario M. The intestinal barrier function and its involvement in digestive disease. *Rev Esp Enferm Dig* 2015; **107**: 686-696 [PMID: 26541659 DOI: 10.17235/reed.2015.3846/2015]

8 **Alonso C**, Vicario M, Pigrau M, Lobo B, Santos J. Intestinal barrier function and the brain-gut axis. *Adv Exp Med Biol* 2014; **817**: 73-113 [PMID: 24997030 DOI: 10.1007/978-1-4939-0897-4_4]

9 **Pongkorpsakol P**, Satitsri S, Wongkrasant P, Chittavanich P, Kittayaruksakul S, Srimanote P, Chatsudthipong V, Muanprasat C. Flufenamic acid protects against intestinal fluid secretion and barrier leakage in a mouse model of Vibrio cholerae infection through NF-κB inhibition and AMPK activation. *Eur J Pharmacol* 2017; **798**: 94-104 [PMID: 28119077 DOI: 10.1016/j.ejphar.2017.01.026]

10 **Ye X**, Sun M. AGR2 ameliorates tumor necrosis factor-α-induced epithelial barrier dysfunction *via* suppression of NF-κB p65-mediated MLCK/p-MLC pathway activation. *Int J Mol Med* 2017; **39**: 1206-1214 [PMID: 28339048 DOI: 10.3892/ijmm.2017.2928]

11 **Lee JY**, Kim EH, Yoon JH, Eo W, Yoon SW. Traditional Herbal Medicine, Sipjeondaebo-Tang, for Cancer-Related Fatigue: A Randomized, Placebo-Controlled, Preliminary Study. *Integr Cancer Ther* 2021; **20**: 15347354211040830 [PMID: 34672230 DOI: 10.1177/15347354211040830]

12 **Morishige KI**. Traditional herbal medicine, Rikkunshito, for chemotherapy-induced nausea and vomiting. *J Gynecol Oncol* 2017; **28**: e57 [PMID: 28657219 DOI: 10.3802/jgo.2017.28.e57]

13 **Jiang HZ**, Jiang YL, Yang B, Long FX, Yang Z, Tang DX. Traditional Chinese medicines and capecitabine-based chemotherapy for colorectal cancer treatment: A meta-analysis. *Cancer Med* 2023; **12**: 236-255 [PMID: 35650714 DOI: 10.1002/cam4.4896]

14 **Huang J**, Zhang J, Sun C, Yang R, Sheng M, Hu J, Kai G, Han B. Adjuvant role of Salvia miltiorrhiza bunge in cancer chemotherapy: A review of its bioactive components, health-promotion effect and mechanisms. *J Ethnopharmacol* 2024; **318**: 117022 [PMID: 37572929 DOI: 10.1016/j.jep.2023.117022]

15 **Nawaz S**, Muhammad Irfan H, Alamgeer, Akram M, Jahan S. Linalool: Monoterpene alcohol effectiveness in chronic synovitis through lowering Interleukin-17, spleen and thymus indices. *Int Immunopharmacol* 2023; **121**: 110517 [PMID: 37348232 DOI: 10.1016/j.intimp.2023.110517]

16 **Rizzo A**, Ricci AD. Challenges and Future Trends of Hepatocellular Carcinoma Immunotherapy. *Int J Mol Sci* 2022; **23** [PMID: 36232663 DOI: 10.3390/ijms231911363]

17 **Rizzo A**, Ricci AD, Brandi G. Systemic adjuvant treatment in hepatocellular carcinoma: tempted to do something rather than nothing. *Future Oncol* 2020; **16**: 2587-2589 [PMID: 32772560 DOI: 10.2217/fon-2020-0669]

18 **Rizzo A**, Brandi G. Biochemical predictors of response to immune checkpoint inhibitors in unresectable hepatocellular carcinoma. *Cancer Treat Res Commun* 2021; **27**: 100328 [PMID: 33549983 DOI: 10.1016/j.ctarc.2021.100328]

19 **Rizzo A**, Dadduzio V, Ricci AD, Massari F, Di Federico A, Gadaleta-Caldarola G, Brandi G. Lenvatinib plus pembrolizumab: the next frontier for the treatment of hepatocellular carcinoma? *Expert Opin Investig Drugs* 2022; **31**: 371-378 [PMID: 34167433 DOI: 10.1080/13543784.2021.1948532]

20 **Rizzo A**, Ricci AD, Brandi G. Trans-Arterial Chemoembolization Plus Systemic Treatments for Hepatocellular Carcinoma: An Update. *J Pers Med* 2022; **12** [PMID: 36579504 DOI: 10.3390/jpm12111788]

21 **Amalia E**, Diantini A, Endang Prabandari E, Waluyo D, Subarnas A. Caffeic Acid Phenethyl Ester as a DHODH Inhibitor and Its Synergistic Anticancer Properties in Combination with 5-Fluorouracil in a Breast Cancer Cell Line. *J Exp Pharmacol* 2022; **14**: 243-253 [PMID: 35910085 DOI: 10.2147/JEP.S365159]

22 **Sakai H**, Sagara A, Matsumoto K, Jo A, Hirosaki A, Takase K, Sugiyama R, Sato K, Ikegami D, Horie S, Matoba M, Narita M. Neutrophil recruitment is critical for 5-fluorouracil-induced diarrhea and the decrease in aquaporins in the colon. *Pharmacol Res* 2014; **87**: 71-79 [PMID: 24972040 DOI: 10.1016/j.phrs.2014.05.012]

23 **Jiang WG**, Ye L, Ruge F, Owen S, Martin T, Sun PH, Sanders AJ, Lane J, Satherley L, Weeks HP, Gao Y, Wei C, Wu Y, Mason MD. YangZheng XiaoJi exerts anti-tumour growth effects by antagonising the effects of HGF and its receptor, cMET, in human lung cancer cells. *J Transl Med* 2015; **13**: 280 [PMID: 26310485 DOI: 10.1186/s12967-015-0639-1]

24 **Wang YX**. [Effect of Yangzheng Xiaoji Capsule Treatment on Patients with Advanced Gastrointestinal Tumors on the Quality of Life and Syndrome]. *Xitong Yixue* 2021; **6**: 56-58 [DOI: 10.19368/j.cnki.2096-1782.2021.10.056]

25 **Schoultz I**, Keita ÅV. The Intestinal Barrier and Current Techniques for the Assessment of Gut Permeability. *Cells* 2020; **9** [PMID: 32824536 DOI: 10.3390/cells9081909]

26 **Haas AJ**, Zihni C, Krug SM, Maraspini R, Otani T, Furuse M, Honigmann A, Balda MS, Matter K. ZO-1 Guides Tight Junction Assembly and Epithelial Morphogenesis *via* Cytoskeletal Tension-Dependent and -Independent Functions. *Cells* 2022; **11** [PMID: 36497035 DOI: 10.3390/cells11233775]

27 **He S**, Liu G, Zhu X. Human breast milk-derived exosomes may help maintain intestinal epithelial barrier integrity. *Pediatr Res* 2021; **90**: 366-372 [PMID: 33731816 DOI: 10.1038/s41390-021-01449-y]

28 **Rawat M**, Nighot M, Al-Sadi R, Gupta Y, Viszwapriya D, Yochum G, Koltun W, Ma TY. IL1B Increases Intestinal Tight Junction Permeability by Up-regulation of MIR200C-3p, Which Degrades Occludin mRNA. *Gastroenterology* 2020; **159**: 1375-1389 [PMID: 32569770 DOI: 10.1053/j.gastro.2020.06.038]

29 **Ibrahim S**, Zhu X, Luo X, Feng Y, Wang J. PIK3R3 regulates ZO-1 expression through the NF-kB pathway in inflammatory bowel disease. *Int Immunopharmacol* 2020; **85**: 106610 [PMID: 32473571 DOI: 10.1016/j.intimp.2020.106610]

30 **Tsukita S**, Tanaka H, Tamura A. The Claudins: From Tight Junctions to Biological Systems. *Trends Biochem Sci* 2019; **44**: 141-152 [PMID: 30665499 DOI: 10.1016/j.tibs.2018.09.008]

31 **Su X**, Wei J, Qi H, Jin M, Zhang Q, Zhang Y, Zhang C, Yang R. LRRC19 Promotes Permeability of the Gut Epithelial Barrier Through Degrading PKC-ζ and PKCι/λ to Reduce Expression of ZO1, ZO3, and Occludin. *Inflamm Bowel Dis* 2021; **27**: 1302-1315 [PMID: 33501933 DOI: 10.1093/ibd/izaa354]

32 **Kumar A**, Priyamvada S, Ge Y, Jayawardena D, Singhal M, Anbazhagan AN, Chatterjee I, Dayal A, Patel M, Zadeh K, Saksena S, Alrefai WA, Gill RK, Zadeh M, Zhao N, Mohamadzadeh M, Dudeja PK. A Novel Role of SLC26A3 in the Maintenance of Intestinal Epithelial Barrier Integrity. *Gastroenterology* 2021; **160**: 1240-1255.e3 [PMID: 33189700 DOI: 10.1053/j.gastro.2020.11.008]

33 **Chelakkot C**, Ghim J, Rajasekaran N, Choi JS, Kim JH, Jang MH, Shin YK, Suh PG, Ryu SH. Intestinal Epithelial Cell-Specific Deletion of PLD2 Alleviates DSS-Induced Colitis by Regulating Occludin. *Sci Rep* 2017; **7**: 1573 [PMID: 28484281 DOI: 10.1038/s41598-017-01797-y]

34 **Johansson ME**, Jakobsson HE, Holmén-Larsson J, Schütte A, Ermund A, Rodríguez-Piñeiro AM, Arike L, Wising C, Svensson F, Bäckhed F, Hansson GC. Normalization of Host Intestinal Mucus Layers Requires Long-Term Microbial Colonization. *Cell Host Microbe* 2015; **18**: 582-592 [PMID: 26526499 DOI: 10.1016/j.chom.2015.10.007]

35 **Kang Y**, Park H, Choe BH, Kang B. The Role and Function of Mucins and Its Relationship to Inflammatory Bowel Disease. *Front Med (Lausanne)* 2022; **9**: 848344 [PMID: 35602503 DOI: 10.3389/fmed.2022.848344]

36 **Arike L**, Holmén-Larsson J, Hansson GC. Intestinal Muc2 mucin O-glycosylation is affected by microbiota and regulated by differential expression of glycosyltranferases. *Glycobiology* 2017; **27**: 318-328 [PMID: 28122822 DOI: 10.1093/glycob/cww134]

37 **Doron I**, Mesko M, Li XV, Kusakabe T, Leonardi I, Shaw DG, Fiers WD, Lin WY, Bialt-DeCelie M, Román E, Longman RS, Pla J, Wilson PC, Iliev ID. Mycobiota-induced IgA antibodies regulate fungal commensalism in the gut and are dysregulated in Crohn's disease. *Nat Microbiol* 2021; **6**: 1493-1504 [PMID: 34811531 DOI: 10.1038/s41564-021-00983-z]

38 **Li Y**, Jin L, Chen T. The Effects of Secretory IgA in the Mucosal Immune System. *Biomed Res Int* 2020; **2020**: 2032057 [PMID: 31998782 DOI: 10.1155/2020/2032057]

39 **Vandeputte D**, Falony G, Vieira-Silva S, Tito RY, Joossens M, Raes J. Stool consistency is strongly associated with gut microbiota richness and composition, enterotypes and bacterial growth rates. *Gut* 2016; **65**: 57-62 [PMID: 26069274 DOI: 10.1136/gutjnl-2015-309618]

40 **Hills RD Jr**, Pontefract BA, Mishcon HR, Black CA, Sutton SC, Theberge CR. Gut Microbiome: Profound Implications for Diet and Disease. *Nutrients* 2019; **11** [PMID: 31315227 DOI: 10.3390/nu11071613]

41 **Scheithauer TPM**, Rampanelli E, Nieuwdorp M, Vallance BA, Verchere CB, van Raalte DH, Herrema H. Gut Microbiota as a Trigger for Metabolic Inflammation in Obesity and Type 2 Diabetes. *Front Immunol* 2020; **11**: 571731 [PMID: 33178196 DOI: 10.3389/fimmu.2020.571731]

42 **Aron-Wisnewsky J**, Warmbrunn MV, Nieuwdorp M, Clément K. Metabolism and Metabolic Disorders and the Microbiome: The Intestinal Microbiota Associated With Obesity, Lipid Metabolism, and Metabolic Health-Pathophysiology and Therapeutic Strategies. *Gastroenterology* 2021; **160**: 573-599 [PMID: 33253685 DOI: 10.1053/j.gastro.2020.10.057]

43 **Wertman JN**, Dunn KA, Kulkarni K. The impact of the host intestinal microbiome on carcinogenesis and the response to chemotherapy. *Future Oncol* 2021; **17**: 4371-4387 [PMID: 34448411 DOI: 10.2217/fon-2021-0087]

44 **Galeano Niño JL**, Wu H, LaCourse KD, Kempchinsky AG, Baryiames A, Barber B, Futran N, Houlton J, Sather C, Sicinska E, Taylor A, Minot SS, Johnston CD, Bullman S. Effect of the intratumoral microbiota on spatial and cellular heterogeneity in cancer. *Nature* 2022; **611**: 810-817 [PMID: 36385528 DOI: 10.1038/s41586-022-05435-0]

45 **Engevik MA**, Danhof HA, Ruan W, Engevik AC, Chang-Graham AL, Engevik KA, Shi Z, Zhao Y, Brand CK, Krystofiak ES, Venable S, Liu X, Hirschi KD, Hyser JM, Spinler JK, Britton RA, Versalovic J. Fusobacterium nucleatum Secretes Outer Membrane Vesicles and Promotes Intestinal Inflammation. *mBio* 2021; **12** [PMID: 33653893 DOI: 10.1128/mBio.02706-20]

46 **Qu Y**, Li X, Xu F, Zhao S, Wu X, Wang Y, Xie J. Kaempferol Alleviates Murine Experimental Colitis by Restoring Gut Microbiota and Inhibiting the LPS-TLR4-NF-κB Axis. *Front Immunol* 2021; **12**: 679897 [PMID: 34367139 DOI: 10.3389/fimmu.2021.679897]

47 **Wu L**, Xi Y, Yan M, Sun C, Tan J, He J, Li H, Wang D. Berberine-Based Carbon Quantum Dots Improve Intestinal Barrier Injury and Alleviate Oxidative Stress in C57BL/6 Mice with 5-Fluorouracil-Induced Intestinal Mucositis by Enhancing Gut-Derived Short-Chain Fatty Acids Contents. *Molecules* 2023; **28** [PMID: 36903391 DOI: 10.3390/molecules28052148]

48 **Fawad JA**, Luzader DH, Hanson GF, Moutinho TJ Jr, McKinney CA, Mitchell PG, Brown-Steinke K, Kumar A, Park M, Lee S, Bolick DT, Medlock GL, Zhao JY, Rosselot AE, Chou CJ, Eshleman EM, Alenghat T, Hong CI, Papin JA, Moore SR. Histone Deacetylase Inhibition by Gut Microbe-Generated Short-Chain Fatty Acids Entrains Intestinal Epithelial Circadian Rhythms. *Gastroenterology* 2022; **163**: 1377-1390.e11 [PMID: 35934064 DOI: 10.1053/j.gastro.2022.07.051]

49 **Cai G**, Yang Y, Gu P, Li K, Adelijiang W, Zhu T, Liu Z, Wang D. The secretion of sIgA and dendritic cells activation in the intestinal of cyclophosphamide-induced immunosuppressed mice are regulated by Alhagi honey polysaccharides. *Phytomedicine* 2022; **103**: 154232 [PMID: 35675749 DOI: 10.1016/j.phymed.2022.154232]

50 **Wang X**, Meng G, Zhang S, Liu X. A Reactive (1)O2 - Responsive Combined Treatment System of Photodynamic and Chemotherapy for Cancer. *Sci Rep* 2016; **6**: 29911 [PMID: 27443831 DOI: 10.1038/srep29911]

51 **Srivastava A**, Gupta J, Kumar S, Kumar A. Gut biofilm forming bacteria in inflammatory bowel disease. *Microb Pathog* 2017; **112**: 5-14 [PMID: 28942174 DOI: 10.1016/j.micpath.2017.09.041]

52 **Wu S**, Rhee KJ, Albesiano E, Rabizadeh S, Wu X, Yen HR, Huso DL, Brancati FL, Wick E, McAllister F, Housseau F, Pardoll DM, Sears CL. A human colonic commensal promotes colon tumorigenesis *via* activation of T helper type 17 T cell responses. *Nat Med* 2009; **15**: 1016-1022 [PMID: 19701202 DOI: 10.1038/nm.2015]

53 **Davis ME**, Lisowyj MP, Zhou L, Wisecarver JL, Gulizia JM, Shostrom VK, Naud N, Corpet DE, Mirvish SS. Induction of colonic aberrant crypts in mice by feeding apparent N-nitroso compounds derived from hot dogs. *Nutr Cancer* 2012; **64**: 342-349 [PMID: 22293095 DOI: 10.1080/01635581.2012.650777]

54 **Wu M**, Xiao H, Liu G, Chen S, Tan B, Ren W, Bazer FW, Wu G, Yin Y. Glutamine promotes intestinal SIgA secretion through intestinal microbiota and IL-13. *Mol Nutr Food Res* 2016; **60**: 1637-1648 [PMID: 27005687 DOI: 10.1002/mnfr.201600026]

Published by **Baishideng Publishing Group Inc**
7041 Koll Center Parkway, Suite 160, Pleasanton, CA 94566, USA
Telephone: +1-925-3991568
E-mail: office@baishideng.com
Help Desk: https://www.f6publishing.com/helpdesk
https://www.wjgnet.com